# NAVAL POSTGRADUATE SCHOOL

## Monterey, California


# THESIS

**ENVIRONMENTAL INFLUENCE ON SHALLOW WATER BOTTOM REVERBERATION**

by

Boon Chuan, Lee

March 2002

| | |
|---|---|
| Thesis Advisor: | Kevin B. Smith |
| Second Reader: | Alan B. Coppens |

**Approved for public release; distribution is unlimited**

THIS PAGE INTENTIONALLY LEFT BLANK

| REPORT DOCUMENTATION PAGE | | | Form Approved OMB No. 0704-0188 |
|---|---|---|---|
| Public reporting burden for this collection of information is estimated to average 1 hour per response, including the time for reviewing instruction, searching existing data sources, gathering and maintaining the data needed, and completing and reviewing the collection of information. Send comments regarding this burden estimate or any other aspect of this collection of information, including suggestions for reducing this burden, to Washington headquarters Services, Directorate for Information Operations and Reports, 1215 Jefferson Davis Highway, Suite 1204, Arlington, VA 22202-4302, and to the Office of Management and Budget, Paperwork Reduction Project (0704-0188) Washington DC 20503. | | | |
| **1. AGENCY USE ONLY** *(Leave blank)* | **2. REPORT DATE** March 2002 | **3. REPORT TYPE AND DATES COVERED** Master's Thesis | |
| **4. TITLE AND SUBTITLE**: Title (Mix case letters)<br>Environmental Influence On Shallow Water Bottom Reverberation | | | **5. FUNDING NUMBERS** |
| **6. AUTHOR(S)** Boon Chuan, Lee | | | |
| **7. PERFORMING ORGANIZATION NAME(S) AND ADDRESS(ES)**<br>Naval Postgraduate School<br>Monterey, CA 93943-5000 | | | **8. PERFORMING ORGANIZATION REPORT NUMBER** |
| **9. SPONSORING /MONITORING AGENCY NAME(S) AND ADDRESS(ES)**<br>N/A | | | **10. SPONSORING/MONITORING AGENCY REPORT NUMBER** |
| **11. SUPPLEMENTARY NOTES** The views expressed in this thesis are those of the author and do not reflect the official policy or position of the Department of Defense or the U.S. Government. | | | |
| **12a. DISTRIBUTION / AVAILABILITY STATEMENT**<br>Approved for public release; distribution is unlimited. | | | **12b. DISTRIBUTION CODE** |


**13. ABSTRACT** ***(maximum 200 words)***

In this work, the influences of various environmental scenarios on the bottom interface and volume reverberation in shallow water were numerically analyzed. Based on similar modeling reverberation geometry defined in previous works, the numerical analyses were conducted for broadband pulse signals to generate complex reverberation structures in the time-domain. The reverberation model used is based on the well-documented Parabolic Equation (PE) approximation. The environmental scenarios are divided into three main categories. They include different sound speed profiles, different levels of bottom interface roughness and different bottom volume fluctuations. While one category is being analyzed, the other two are held constant. The various analyses include broadband two-way reverberation levels comparisons, vertical correlation analysis and power spectral analysis.


| **14. SUBJECT TERMS**<br>Shallow water reverberation, reverberation pressure levels, coherence, peak vertical correlations, power spectral density, power ratio spectral density, MMPE. | | | **15. NUMBER OF PAGES** 69<br>**16. PRICE CODE** |
|---|---|---|---|
| **17. SECURITY CLASSIFICATION OF REPORT** Unclassified | **18. SECURITY CLASSIFICATION OF THIS PAGE** Unclassified | **19. SECURITY CLASSIFICATION OF ABSTRACT** Unclassified | **20. LIMITATION OF ABSTRACT** UL |

NSN 7540-01-280-5500 Standard Form 298 (Rev. 2-89)
Prescribed by ANSI Std. 239-18

THIS PAGE INTENTIONALLY LEFT BLANK

**Approved for public release; distribution is unlimited**

# ENVIRONMENTAL INFLUENCE ON SHALLOW WATER BOTTOM REVERBERATION

Boon Chuan, Lee
Major, Republic of Singapore Navy
B.Eng.(Hons), King's College, University Of London, U.K. 1992

Submitted in partial fulfillment of the
requirements for the degree of

**MASTER OF SCIENCE IN ENGINEERING ACOUSTICS**

from the

**NAVAL POSTGRADUATE SCHOOL**
**March 2002**

Author: Boon Chuan, Lee

Approved by: Kevin B. Smith, Thesis Advisor

Alan B. Coppens, Second Reader

Kevin B. Smith, Chairman
Engineering Acoustics Academic Committee

THIS PAGE INTENTIONALLY LEFT BLANK

# ABSTRACT

In this work, the influences of various environmental scenarios on the bottom interface and volume reverberation in shallow water were numerically analyzed. Based on similar modeling reverberation geometry defined in previous works, the numerical analyses were conducted for broadband pulse signals to generate complex reverberation structures in the time-domain. The reverberation model used is based on the well-documented Parabolic Equation (PE) approximation. The environmental scenarios are divided into three main categories. They include different sound speed profiles, different levels of bottom interface roughness and different bottom volume fluctuations. While one category is being analyzed, the other two are held constant. The various analyses include broadband two-way reverberation levels comparisons, vertical correlation analysis and power spectral analysis.

THIS PAGE INTENTIONALLY LEFT BLANK

# TABLE OF CONTENTS

# LIST OF FIGURES

# LIST OF TABLES

THIS PAGE INTENTIONALLY LEFT BLANK

# ACKNOWLEDGMENTS

The eighteen months of education received at the Naval Postgraduate School have been very fulfilling and rewarding. The knowledge gained during the period has broadened my horizons, especially in the underwater acoustic field. Working on the thesis has given me an opportunity to apply what I have learned. However, the successful completion of my thesis would not be possible without the support of the following people.

First, I would like to thank Rachel, my wife, for giving me all the possible encouragement and motivation that one would ever want, especially during the last quarter of my course. She took care of all the packing and pre-departure matters, thus allowing me full concentration on my studies and thesis.

Special thanks go to Professor Kevin Smith, my thesis advisor for his patience and guidance throughout the tenure of my thesis work.

My appreciation to Professor Alan Coppens, the thesis second reader for his time and advise.

Last but not least, my gratitude also goes to CDR Jim Hill (USW Curricular Officer), Professor James Sanders (Academic Associate), Eva Anderson (USW Educational Technician) and the Faculty and Staff of the Physics Department.

THIS PAGE INTENTIONALLY LEFT BLANK

# I. INTRODUCTION

As the Navy expands its operations towards the littoral region, the ability to accurately characterize reverberation in shallow water becomes extremely important. Shallow water reverberation affects active sonar systems, impacting the performance of underwater detection and tracking systems, as well as acoustic communications. The primary mechanisms creating shallow water acoustic reverberation are the propagation, the bottom interface and sub-bottom fluctuations, and the rough sea surface.

In the early 1990's, the Office of Naval Research (ONR) sponsored a multi-year reverberation program known as the Acoustic Reverberation Special Research Project (ARSRP). The main goal was to study the primary causes and nature of acoustic reverberation in the deep ocean. The area examined was near the Mid-Atlantic Ridge, an area where the bottom is covered mostly by highly variable topography and hard rock structures. The results from the experiments showed that the predominant mechanism for high reverberation levels was the interaction of the propagation with the bottom interface topography, with harder rocks generating higher scattering levels than softer sediment ponds. To a great extent, the general structure of the reverberation coincided well with the predicted two-way transmission loss, with high reverberation returns occurring at areas where the acoustic energy interacted strongly with the bottom. This implied that much of the long wavelength statistics of the acoustic energy could be predicted by using propagation modeling.

ONR has recently sponsored another reverberation study within a program codenamed ASIAEX, to record reverberation signals and collect oceanographic data in the shallow waters of East China Sea. In contrast to the deep ocean reverberation experiment, the seabed of this littoral region has a much smoother, softer and more penetrable bottom layer such as sand or mud, covering a harder sub-bottom layer of coarser sand, gravels or rocks.

For the past few years, thesis work by previous students[1],[2] was focused on examining the shallow water bottom reverberation using the Monterey-Miami Parabolic Equation (MMPE) propagation model.[3] The MMPE model was first developed by

Smith and Tappert in 1994. Since then, the MMPE model has been further improved to include bottom interface and volume perturbations in order to create more realistic environmental models. The interface perturbation is simply a spatial displacement perturbation while the volume perturbation involves both sound speed and density fluctuations within the sediment.

The previous work modeled a 16-element vertical line array (VLA) geometry to support monostatic and bistatic (vertical separation) reverberation computation in a shallow water environment. The element located at 48m was chosen as the source with all 16 elements acting as receiver. The previous environment was a 100m isospeed water column with a single water/bottom interface. The bottom was modeled with an interface root-mean-square (rms) roughness of 1m and a 15m/s rms volume sound speed perturbation. With the geometry and environmental parameters defined, several reverberation analyses were then conducted to compare perturbed data with and without density fluctuations in the environment for both continuous wave (CW) and broadband signals. The analyses included reverberation pressure level comparisons, vertical correlation analysis, peak correlation analysis and spectral analysis. Some of the significant results were as follows:

- The influence of volume density fluctuations was to reduce later reverberation levels relative to earlier levels but did not affect the structure significantly. This was due to the direct correlation between volume sound speed and density fluctuations used in the model.
- It was noted that the CW analysis was unable to capture coherent structure of the volume reverberation pressure level due to the inability of CW to resolve multi-path influence. Therefore, the peak vertical correlation analysis was valid only for broadband pulse computations.
- The peak vertical correlation analysis suggested that the volume reverberation decorrelated across the vertical array more rapidly than interface reverberation. This was presumably due to multi-point/multi-depth scatter contributions of the volume producing more vertical structure than the interface.

- Spectral analysis of both CW and broadband pulse calculations suggested that response of the interface reverberation has a slope on the order of –0.125 for both CW and broadband data. However, the volume response showed a steeper –0.75 slope for CW and –0.25 slope for broadband signals.

Taking into consideration the findings obtained from previous work, the objective of this thesis is to examine the influence of various environmental profiles on the character of the predicted bottom reverberation for broadband signals. The MMPE model was used to generate the bottom reverberation data, using the same 16-element VLA reverberation geometry defined previously. The MMPE model application program used is named "MMPEREVERBDENS2" and is written in the FOTRAN programming language. The environmental models used include different sound speed profiles and two bottom interfaces (water/bottom interface and bottom/sub-bottom interface) with different interface roughness and volume perturbation. The sound speed profiles were based on data taken during the recent East China Sea portion of ASIAEX, while the bottom and sub-bottom characterization were based on preliminary reports of the geo-acoustics of the region[4]. Signal processing and analysis in the time domain were performed using MATLAB. Data comparisons were made then with reference to reverberation results generated using an environmental profile typical of a shallow water region.

THIS PAGE INTENTIONALLY LEFT BLANK

# II. NUMERICAL METHODS AND IMPLEMENTATION

## A. REVERBERATION THEORY

Reverberation arises from the scattering or re-radiation of the transmitted signals from unwanted targets such as marine life, bubbles, the sea surface, sea bottom and sub-bottom fluctuations. The focus in this thesis is to examine the reverberation generated by the water/bottom interface, bottom/sub-bottom interface and the bottom volume fluctuations in shallow water. The sea bottom interface variability ranges from small features producing Bragg scatter to large features such as sea mounts and pinnacles producing mostly specular reflection of larger wavelengths.

The theoretical principle of the scattering mechanism is the same for both monostatic or bistatic reverberation. The theoretical treatment will only focus on the monostatic mode since its numerical implementation is simpler.

In decibel units relative to 1 μPa and reference length scale of 1 m, we define the *mean reverberation pressure level*, *RPL*, as [1]

$$RPL = 10\log\left[\left\langle \frac{\left|p_{-}^{2}\right|}{p_{ref}^{2}} \right\rangle\right] = SL + DI_T + DI_R + 10\log\left[\frac{\Delta A_b}{R_0^2}\right] - RL_{b,v}, \qquad (2.1)$$

where $SL$ is the source level, $DI_T$ is the directivity index for the transmitter, $DI_R$ is the directivity index for the receiver, $\Delta A_b$ is the ensonified area in the horizontal direction, $R_0$ is the reference distance, and $RL_{b,v}$ is the *reverberation loss* per unit area for either the bottom interface or the volume.

### 1. Bottom Interface Scattering

The reverberation loss for the bottom interface is defined by[1]

$$RL_b = 2TL_b - S_b \tag{2.2}$$

and

$$S_b = 10\log\left[\frac{k_0^2}{32p^2}\left(\frac{\Delta c}{c_0}\right)^2 W_s(2k_0)\right], \tag{2.3}$$

where $TL_b$ is the average transmission loss (based on long wavelength components) from source to the scattering patch at the bottom, $S_b$ is the full-wave scattering strength due to the small-scale interface roughness, $k_0$ is the wavenumber, $c_0$ is a reference sound speed, $\Delta c$ is the difference in sound speed between the water and the bottom at the interface, and $W_s(2k_0)$ is the two-dimensional (2-D) spectrum of the interface roughness evaluated at the Bragg wavenumber for monostatic reverberation.

### 2. Volume Scattering

The volume reverberation loss cannot be expressed simply in terms of the two-way transmission loss but instead must be the integral over depth of the quantity $\left\langle \hat{n}(r,z)\left|y(r,z)\right|^2\right\rangle^2$ at each range r, where $\hat{n}(r,z)$ is the approximate refractive index based on only long wavelength perturbation, and $y(r,z)$ is the field function of the two-way propagation (as defined in Eq 2.11). The reverberation loss for the volume is then defined by[1]

$$RL_v = -20\log\left[\frac{1}{r}\int_{z_b+h_l}^{\infty} \hat{n}(r,z)\left|y(r,z)\right|^2 dz\right] - S_v \tag{2.4}$$

and

$$S_v = 10\log\left[\frac{k_0^2}{32p^2} W_{2s}(2k_0)\right], \tag{2.5}$$

where $S_v$ is the volume scattering strength, $W_{2s}(2k_0)$ is the 2-D horizontal spectrum of the volume fluctuations, which is assumed horizontally isotropic and independent of depth evaluated at the Bragg wavenumber.

## B. MONTEREY-MIAMI PARABOLIC EQUATION (MMPE) MODEL

The parabolic equation (PE) method is a popular numerical approach for solving the acoustic wave equation. The MMPE Model[3] is based upon the parabolic approximation of the wave equation and, therefore, a brief description of this approach would be useful.

We start by representing the time harmonic acoustic pressure field defined in a cylindrical coordinate system and assuming azimuthal symmetry,

$$P(r,z,wt) = p(r,z)e^{-iwt}. \tag{2.6}$$

Cylindrical coordinate is chosen because the shallow water sea can be portrayed as a thin waveguide on the surface of the earth. Azimuthal symmetry is assumed because the ocean environment tends to exhibit weak azimuthal dependence. Substituting Eq. (2.6) into the wave equation in cylindrical coordinates leads to the Helmholtz equation,

$$\nabla^2 p(r,z) + \frac{w^2}{c(r,z)^2} p(r,z) = 0, \tag{2.7}$$

where

$$\nabla^2 = \frac{1}{r}\frac{\partial}{\partial r} r \frac{\partial}{\partial r} + \frac{\partial^2}{\partial z^2}. \tag{2.8}$$

The Helmholtz equation can be factored by introducing the operator notation

$$Q_{op} = (m + e + 1)^{\frac{1}{2}}, \tag{2.9}$$

where

$$e = n^2 - 1, \quad n = \frac{c_0}{c} \quad \text{and} \quad m = \frac{1}{k_o^2}\frac{\partial^2}{\partial z^2}, \tag{2.10}$$

and $c_0$ is the reference sound speed typical of the ocean volume.

Taking into consideration the effect of cylindrical spreading, and proper factorization of the Helmholtz equation, the acoustic pressure may then be defined as,

$$p(r,z) = P_o \sqrt{\frac{R_o}{r}} Q_{op}^{-1/2} y\,(r,z) e^{ik_o r}\ , \tag{2.11}$$

where $y(r,z)$ is the envelope function or PE field function. The parabolic equation for the field function is then defined by

$$\frac{\partial y}{\partial r} = -ik_o y + ik_o Q_{op} y = -ik_o H_{op} y\ , \tag{2.12}$$

where

$$H_{op} = 1 - Q_{op} \tag{2.13}$$

is a Hamiltonian-like operator which defines the evolution of the PE field function in range.

The relationship between values of $y$ at different ranges can be defined by

$$y\,(r+\Delta r) = \Phi(r) y\,(r), \tag{2.14}$$

where $\Phi(r)$ is a propagator that marches the solution out in range. The MMPE model employs a split-step Fourier (PE/SSF) method[5] to provide a representation of the propagator $\Phi(r)$. This method is utilized primarily because of the speed and simplicity of the PE/SSF method. With the Fast Fourier Transform (FFT), the PE/SSF implementation can be represented by

$$y\,(r+\Delta r, z) = e^{-ik_o \frac{\Delta r}{2} U_{op}(r+\Delta r, z)} FFT\left\{ e^{-ik_o \Delta r \hat{T}_{op}(k_z)} IFFT\left( e^{-ik_o \frac{\Delta r}{2} U_{op}(r,z)} y\,(r,z) \right) \right\}, \tag{2.15}$$

where

$$U_{op} = -[n-1] \tag{2.16}$$

and

$$\hat{T}_{op} = 1 - \left[ 1 - \left( \frac{k_z}{k_o} \right)^2 \right]^{1/2}\ . \tag{2.17}$$

## C. IMPLEMENTATION OF THE REVERBERATION PROBLEM IN MMPE

Having described the concepts of reverberation theory and the MMPE model, we will now focus on the theoretical treatments for generating perturbation to both interface roughness and volume sound speed, including the influence of density fluctuations of the volume. The incorporation of these effects into the MMPE model is also discussed. The theoretical basis for modeling the interface roughness is based on the work of Goff and Jordon,[6] and the development for the volume perturbation theory is based on Yamamoto's work.[7]

### 1. Interface Roughness

We assume a two-dimensional (2-D) interface spectrum of the form[1]

$$W_2(k_r) = \frac{m}{(1 + L_{corr}^2 k_r^2)^{b/2}} \text{ and } k_r = \sqrt{K^2 + L^2}\,, \tag{2.18}$$

where $k_r$ is the horizontal spatial wavenumber vector, $m$ is a normalization factor, $L_{corr}$ is a correlation length scale, $b$ is the spectral exponent and $K$ and $L$ are the horizontal wavenumbers in the x- and y-directions, respectively.

If the 2-D spectrum $W_2(k_r)$ is assumed to be independent of direction (isotropic), then the normalization factor $m$ can be defined in terms of the root-mean-square (rms) roughness $s^2$ by requiring

$$2p \int_0^\infty W_2(k_r) k_r dk_r = s^2\,, \tag{2.19}$$

which leads to

$$m = \frac{1}{p}\left(\frac{b}{2} - 1\right) s^2 L_{corr}^2\,. \tag{2.20}$$

We simply evaluate $W_2(k_r)$ at $k_r = 2k_0$ for the scattering amplitude since it is caused by Bragg scatter (evaluated along the line of propagation for monostatic reverberation). However, for the long-wavelength interface roughness, we need the full spectrum, i.e. the one-dimensional (1-D) spectrum along the x-axis. This can be done by taking the 1-D transform of $W_2(K,L)$ along a slice at y=0, defined by

$$W_1(K) = \int_{-\infty}^{\infty} W_2(K,L)dL\,. \tag{2.21}$$

In cylindrical coordinates, we have

$$W_1(K) = 2\int_K^{\infty} \frac{k_r}{\sqrt{k_r^2 - K^2}} W_2(k_r)dk_r = gs^{\,2}L_{corr}(1+L_{corr}^2K^2)^{-\frac{b}{2}+\frac{1}{2}}, \tag{2.22}$$

where

$$g = \frac{\left(\frac{b}{2}-1\right)\Gamma\left(\frac{1}{2}\right)\Gamma\left(\frac{b}{2}-\frac{1}{2}\right)}{p\Gamma\left(\frac{b}{2}\right)}. \tag{2.23}$$

In order to generate a 1-D roughness realization from Eq. (2.21) or Eq. (2.22), we transform the 1-D amplitude spectrum that has been scaled by a random amplitude and phase. That means we can define the roughness realization as

$$h(x) = \int_{-\infty}^{\infty} S_1(K)e^{iKx}dK\,, \tag{2.24}$$

where

$$S_1(K) = \left[W_1(K)\right]^{1/2} A(K)e^{iq(K)} \tag{2.25}$$

and $A$ and $q$ are random numbers for all values of $K$. The random phase and amplitude of each component can be obtained from Eq. (2.26) and Eq. (2.27), respectively

$$q = 2p\,r_1 \tag{2.26}$$

$$A = \sqrt{-\ln(r_2)} \tag{2.27}$$

where both $r_1$ and $r_2$ are independent uniformly distributed random variables in the interval [0,1]. In practice, we simply use

$$W_1(K) = \left(1+L_{corr}^2K^2\right)^{-\frac{b}{2}+\frac{1}{2}} \tag{2.28}$$

and rescale the result by its rms value, i.e. $\dfrac{h(x)}{\left\langle h^2(x)\right\rangle^{\frac{1}{2}}}$.

## 2. Volume Sound Speed Fluctuations

The sediment volume sound speed perturbation may be modelled by a three-dimensional (3-D) volume spectrum given by[1]

$$W_3(K,L,M) = \frac{b\Lambda^2 B}{2p}\left(\Lambda^2\left(K^2 + L^2\right) + M^2\right)^{-\frac{b}{2}-1}, \tag{2.29}$$

where $B$ is the spectral strength constant, $b$ is the spectral exponent, and $\Lambda = \frac{a_3}{a_1} = \frac{a_3}{a_2}$ is the horizontal-to-vertical aspect ratio describing the anisotropy of fluctuations in the sediment, $K$ and $L$ are the horizontal wavenumbers in the x- and y-directions, respectively, and M is the vertical wavenumber.

To evaluate the reverberation due to the volume perturbation, we need an expression for the 2-D *horizontal* spectrum (assuming strongest scattering near horizontal). It is defined as

$$W_2(K,L) = \int_{-\infty}^{\infty} W_3(K,L,M)\,dM\ . \tag{2.30}$$

Substituting Eq.(2.29) into Eq.(2.30), we have

$$W_2(K,L) = \frac{b\Lambda^2 B}{p}\int_0^{\infty}\left[\Lambda^2\left(K^2 + L^2\right) + M^2\right]^{-\frac{b}{2}-1} dM\ . \tag{2.31}$$

For $b = 2$, Eq. (2.31) can be reduced to

$$W_2(K,L) = \frac{\Lambda^2 B}{2}\left[\Lambda^2\left(K^2 + L^2\right)\right]^{-\frac{3}{2}}. \tag{2.32}$$

For the values of $B \sim 5\times10^{-4}$ and $\Lambda \sim 5$ chosen from Yamamoto's findings,[7] Eq. (2.32) reduces to

$$W_2(K,L) = a\left(K^2 + L^2\right)^{-\frac{3}{2}}, \tag{2.33}$$

where

$$a = \frac{B}{2\Lambda} = 5\times 10^{-5}. \tag{2.34}$$

However, for the forward propagation, we need only the 2-D *vertical* spectrum in the $(r, z)$ plane. It can be defined by

$$W_2'(K,M) = \int_{-\infty}^{\infty} W_3(K,L,M)dL = \frac{b\Lambda^2 B}{2p}\int_{-\infty}^{\infty}\left[\Lambda^2\left(K^2+L^2\right)+M^2\right]^{-\frac{(b+2)}{2}}dL. \tag{2.35}$$

For $b = 2$, Eq. (2.35) becomes

$$W_2'(K,M) = a'\left[25K^2+M^2\right]^{-\frac{3}{2}}, \tag{2.36}$$

where

$$a' = 1.25\times 10^{-3}\ . \tag{2.37}$$

To generate 2-D vertical volume sound speed fluctuation realizations, we define a realization as

$$c_0 d(x,z) = \iint S_2(K,M)e^{iKx}e^{iMz}dKdM\ , \tag{2.38}$$

where

$$S_2(K,M) = \left[W_2'(K,M)\right]^{1/2} A(K,M)\,e^{iq(K,M)}\ . \tag{2.39}$$

Notice that since we have treated the sound speed perturbation in the volume in the *vertical*, we are really generating a series of *vertical* realizations at each range step.

In similar fashion to the interface, the 2-D random phase and the amplitude variations can be obtained, respectively, by

$$q(K,M) = 2p\,r_1(K,M) \tag{2.40}$$

and

$$A(K,M) = \sqrt{-\ln(r_2(K,M))} \tag{2.41}$$

where both $r_1(K,M)$ and $r_2(K,M)$ are now a *matrix* of uniformly distributed random numbers in [0,1]. In practice, we use

$$W_2'(K,M) \propto \left(\Lambda^2 K^2 + M^2\right)^{-\frac{b}{2}-1}, \tag{2.42}$$

and rescale by the appropriate rms values.

Eqs. (2.28) and (2.42) are the results for the interface roughness and volume perturbation, respectively. These are the generic spectral models used in generating the realizations for implementation in the MMPE model.

## 3. Density Fluctuations in Sediment

Variability in density, $r$, is incorporated into the PE model by defining the effective index of refraction[8]

$$n'^2 = n^2 + \frac{1}{2k_0^2}\left[\frac{1}{r}\nabla^2 r - \frac{3}{2}\left(\frac{1}{r}\nabla r\right)^2\right]. \tag{2.43}$$

Consistent with the numerical treatment that assumes the environment is range-independent over a range step, and the fact that sediment properties are largely horizontally stratified, we may simplify this to

$$n'^2 = n^2 + \frac{1}{2k_0^2}\left[\frac{1}{r}\frac{\partial^2 r}{\partial z^2} - \frac{3}{2}\left(\frac{1}{r}\frac{\partial r}{\partial z}\right)^2\right]. \tag{2.44}$$

For the forward problem, the sound speed index of refraction is based only on large scale features, such that

$$n_b^2 \to \hat{n}_b^2(\vec{r}, z) = \frac{c_0^2}{\overline{c}_b^2} \tag{2.45}$$

and

$$\overline{c}_b = c_{b_0}(1 + b_z + d_l) = c_{b_0} + dc_b, \quad dc_b = c_{b_0}(b_z + d_l), \tag{2.46}$$

where $c_{b_0}$ is the mean bottom sound speed at the interface, $b_z = g/c_{b_0}$ is the normalized gradient of bottom sound speed, and $d_l$ is the zero-mean random perturbation for the long wavelength component.

According to the analysis of Yamamoto (1996),[7] the relative fluctuations in density relate to the relative fluctuations in sound speed according to

$$\frac{dr}{r_0} = \frac{2(r_r - r_0)}{2r_0 - r_r}\frac{dc}{c_0} = 2g\,\frac{dc}{c_0}, \tag{2.47}$$

where

$$c_0 = c_{b_0}(1 + b_z) \text{ and } g = \frac{r_r - r_0}{2r_0 - r_r}\ . \tag{2.48}$$

Notice that $r_0$ and $c_0$ are the averaged values of the density and sound speed in the sediment and $r_r = 2650\,{kg}/{m^3}$ is the density of the grain. We may then write

$$r = r_0 + dr = r_0\left[1 + \frac{2g}{c_0}dc\right]. \tag{2.49}$$

Taking the first and second partial derivatives of Eq. (2.49) with respect to depth, z, and neglecting depth gradients in either $c_0$ or $r_0$, we obtain

$$\frac{\partial r}{\partial z} = \frac{2gr_0}{c_0}\frac{\partial}{\partial z}(dc) \tag{2.50}$$

and

$$\frac{\partial^2 r}{\partial z^2} = \frac{2gr_0}{c_0}\frac{\partial^2}{\partial z^2}(dc). \tag{2.51}$$

The sound speed fluctuation is defined by

$$dc_b = c_0 d(x,z) = \iint S_2(K,M)e^{iKx}e^{iMz}dKdM\ , \tag{2.52}$$

where

$$S_2(K,M) = \left[W_2'(K,M)\right]^{1/2} A(K,M)\,e^{i\eta(K,M)}. \tag{2.53}$$

Substituting Eq. (2.52) into Eq. (2.50) and Eq. (2.51) yields

$$\frac{\partial r}{\partial z} = \frac{2gr_0}{c_0}\iint (iM)S_2(K,M)e^{iKx}e^{iMz}dKdM \tag{2.54}$$

and

$$\frac{\partial^2 r}{\partial z^2} = \frac{2g r_0}{c_0} \iint \left(-M^2\right) S_2\left(K, M\right) e^{iKx} e^{iMz} dKdM \,. \tag{2.55}$$

The sediment effective index of refraction can now be derived by substituting Eq. (2.54) and Eq. (2.55) into Eq. (2.44), which becomes

$$n_b'^2\left(x, z\right) = n_b^2\left(x, z\right) + \frac{1}{2k_0^2}\left[a\left(x, z\right) + b\left(x, z\right)\right], \tag{2.56}$$

where

$$a\left(x, z\right) = \frac{-2g}{c_0\left(x, z\right)} \iint M^2 S_2\left(K, M\right) e^{iKx} e^{iMz} dKdM \tag{2.57}$$

and

$$b\left(x, z\right) = +3/2\left[\frac{2g}{c_0\left(x, z\right)} \iint M S_2\left(K, M\right) e^{iKx} e^{iMz} dKdM\right]^2. \tag{2.58}$$

These parameters will be computed in parallel with $d\,c_b$ in the MMPE model.

In the sediment, there is then the additional propagator term

$$\Phi_r\left(x, z\right) = e^{i\Delta r k_0 U_r\left(x, z\right)}, \tag{2.59}$$

where

$$U_r\left(x, z\right) = -\frac{1}{4k_0^2}\left[a\left(x, z\right) + b\left(x, z\right)\right]. \tag{2.60}$$

## D. TIME-DOMAIN PROCESSING

The theoretical treatment of the reverberation loss for the bottom interface $RL_b$ and the volume $RL_v$ discussed previously were based on CW analysis. However, our focus here is on broadband analysis. To predict the effect of pulse propagation in time, we need to run the MMPE model over a spectrum of frequencies. This allows us to treat coherent interference effects by separating the multipath effects. The time-domain analysis of the interface and the volume reverberation will provide the general picture of the two-way travel time structure of the reverberation loss. We can then determine the reverberant field at each range step and continue the propagation through the entire water column of interest.

### 1. Time-Domain Analysis of the Interface

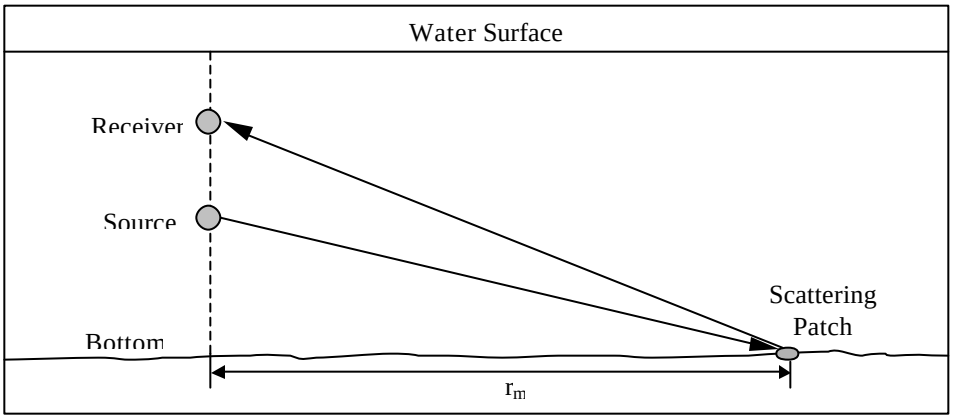


Figure 1. Two-Way Return from a Scattering Patch

The geometry of a *two-way return from a scattering patch* adapted from Smith and Cushman[9] is shown in Figure 1. The travel time structure of the one-way forward propagating field at range step $r_m$ is denoted by $p_+(r_m,z,t)$ where $t = T - \frac{r_m}{c_0}$ is the reduced time and $T$ is the actual travel time. The two-way pressure field at the receiver is the convolution of two, one-way fields in the time-domain[9]

$$p_{2-way,b}(r_m, t) = \int p_{+Tb}(r_m, t)\, p_{+Rb}(r_m, t - t)dt\,, \tag{2.61}$$

where $p_{+Tb}$ and $p_{+Rb}$ are the forward propagated pressure fields from the transmitter and receiver to the scattering point evaluated at the bottom interface, respectively. Note that

here $t = T - \frac{2r_m}{c_0}$ is the reduced time of the reverberation and $T$ is the actual travel time. Furthermore, the receiver and transmitter need not be co-located in the water column. By reciprocity, the propagated field from the receiver to the scattering point, $p_{+Rb}$ is the same as the propagated field from the scattering point to the receiver $p_{-Rb}$.

The time-domain convolution of the two field functions is also the scalar multiplication of these functions in the frequency domain. Hence, the two-way field in the frequency domain from the interface can be expressed as

$$p_{2-way,b}(r_m, f) = p_{+Tb}(r_m, f)\, p_{+Rb}(r_m, f), \tag{2.62}$$

where

$$p_{+Tb}(r_m, f) = \frac{1}{\sqrt{r_m}} y_{+Tb}(r_m, f) e^{i k_0 r} \tag{2.63}$$

and

$$p_{+Rb}(r_m, f) = \frac{1}{\sqrt{r_m}} y_{+Rb}(r_m, f) e^{ik_0 r} \ . \tag{2.64}$$

The two-way travel time structure of the reverberation loss for the bottom interface, $RL_b$, due to a single bottom patch can then be defined as

$$p_{-b}(r_m, t) = A \int p_{2-way,b}(r_m, f) e^{-i2\pi ft} df \ , \tag{2.65}$$

where the constant $A$ is included to incorporate all the other factors needed to define reverberation loss, $RL_b$. This provides the two-way travel time structure due to scattering from range $r_m$. The calculation is then continued for each range step. The total field at the receiver is computed by coherently summing up all the pressure values from the different range segments, $r_m$, by matching up the discrete arrival times, $t_n$, according to

$$p_{-b}(t_n) = \sum_{m=1}^{M} p_{-b}(r_m, t_n), \tag{2.66}$$

where $p_{-b}$ is the total interface reverberation pressure received at the receiver at time $t_n$.

## 2. Time-Domain Analysis of the Volume

The reverberant field due to each depth/range point is computed by combining the source-to-patch and patch-to-receiver propagating field, according to

$$p_{2-way,v}(r_m, z, f) = n(r_m, z)\, p_{+T}(r_m, z, f)\, p_{+R}(r_m, z, f), \tag{2.67}$$

where the two-way reverberation signal is computed for every grid point of interest ($z > z_b$ always) at a particular frequency, $f$, and $n(r_m, z)$ is the local index of refraction at the grid point. The reason for multiplying by the local index of refracttion, $n(r_m, z)$, is to provide the same weighting used in the CW treatment.

Fourier transform gives the time-domain response

$$p_{2-way,v}(r_m, z, t) = B \int p_{2-way,v}(r_m, z, f) e^{-i 2\pi f t} df \ . \tag{2.68}$$

The two-way travel time structure of the reverberation loss for the volume, $RL_v$, can then be derived from

$$p_{-v}(r_m, t) = \int_{z>z_b}^{\infty} p_{2-way,v}(r_m, z, t)\, dz, \tag{2.69}$$

which is the coherent sum over all depths below the interface at range step $m$. Note that the constant $B$ is included to account for all the other terms needed to define reverberation loss, $RL_v$. The single set of time series can then be matched and summed to give

$$p_{-v}(t_n) = \sum_{m=1}^{M} p_{-v}(r_m, t_n), \tag{2.70}$$

where $p_{-v}$ is the two-way time domain pressure defining the volume reverberation loss at the receiver at time, $t_n$, due to the entire volume of interest.

# III. MODELING GEOMETRY & ENVIRONMENT

## A. MULTI-STATIC REVERBERATION GEOMETRY

Since the varying spatial properties of the broadband signal are of interest, a vertical line array (VLA) with 16 elements was chosen. The VLA will support both monostatic and bistatic (in the vertical) reverberation computations/measurements. The array was located vertically in the 100m deep water column and each element of the VLA was assumed to be a point source/receiver. Figure 2 shows the VLA and its geometry relative to a scattering patch at a horizontal range, *r*. From Figure 2, we see that the 16-element VLA spans the water column from 20m to 80m with 4m separation in depth between adjacent elements. A single element located at 48m depth was chosen as the source with all 16 elements receiving the reverberation. To perform broadband analysis, a center frequency of 250Hz was chosen with a 250Hz bandwidth.

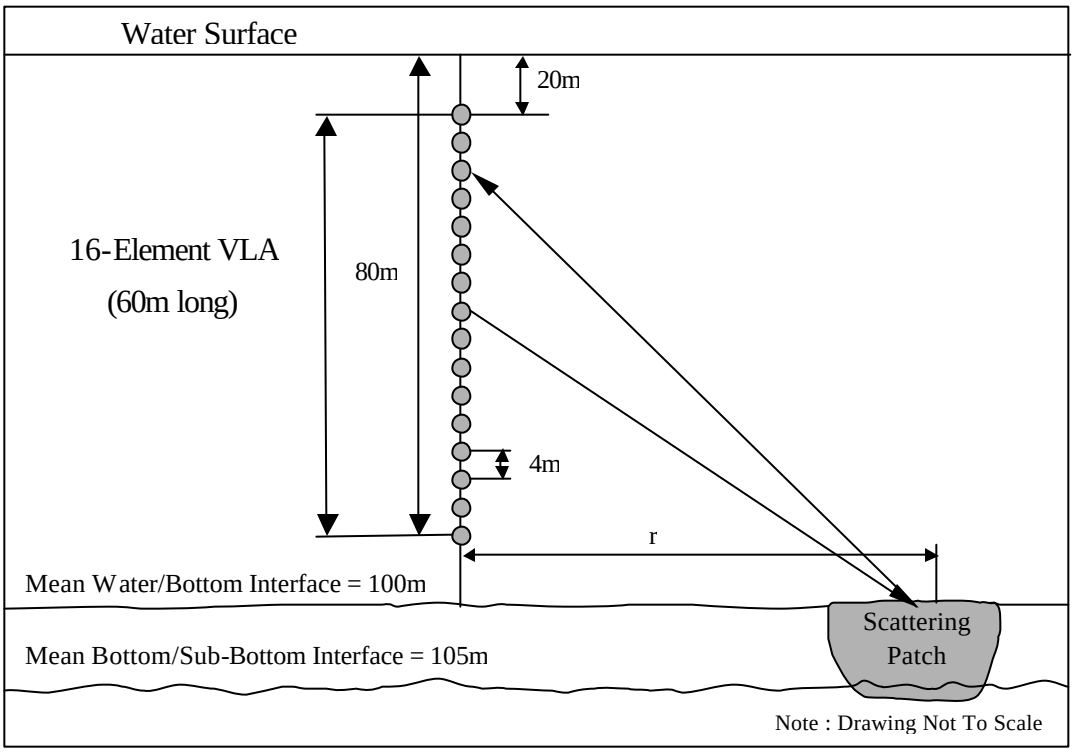


Figure 2. Geometry of VLA and Scattering Patch

## B. THE ENVIRONMENTAL MODELS

The maximum propagation range is 5km. The mean bottom depth is 100m while the mean sub-bottom or deep-bottom depth is 105m. Hence, there are two bottom interfaces, the water/bottom and bottom/sub-bottom (or bottom/deep-bottom) interfaces. This is physically representative of a smoother, softer and more penetrable bottom layer such as sand or mud, covering a harder sub-bottom layer of coarser sand, gravel or rocks.

Seven sets of environmental parameters are used to run the MMPE model. The main differences between each set are the variations in sound speed profiles (SSP) of the water column, water/bottom and bottom/sub-bottom interface roughness and bottom/sub-bottom volume sound speed perturbation. One of the seven profiles is a reference model that follows the typical profiles of what is expected in the shallow water region. The six other models are divided into three categories based on the differences mentioned. Comparison of results within each category will be done with respect to the reference model.

### 1. Variations in Sound Speed Profiles

Six representative sound speed profiles were obtained from the ASIAEX experiments and are plotted in the figure below. Of the six, the two extreme left and right sound speed profiles (SSP1 and SSP2) and the average sound speed profile (SSPAvg) were chosen for the modeling runs. The SSPAvg is used in the reference model.

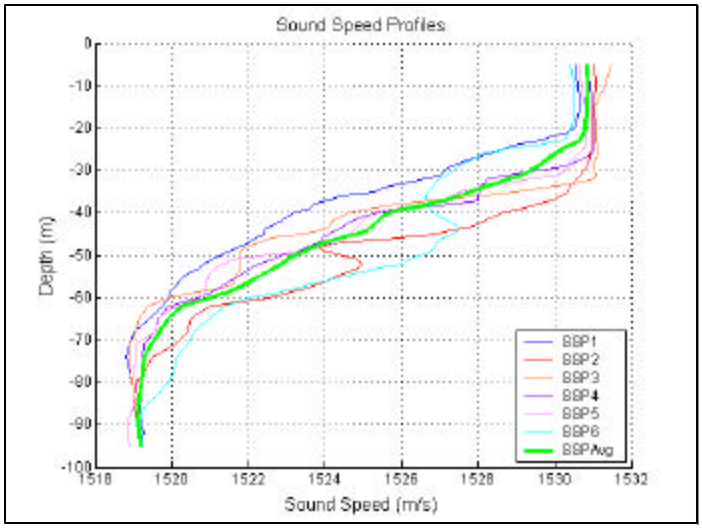


Figure 3. Typical Sound Speed Profiles of East China Sea

## 2. Variations in Interface Roughness

Three sets of interface root-mean-square (rms) roughness are used. They are (0.5m, 1m), (1m, 2m) and (2m, 4m) for each water/bottom and bottom/sub-bottom interface pair. Plots of the rough interface realizations for the bottom and sub-bottom bathymetry for different rms values are shown in Figure 4.

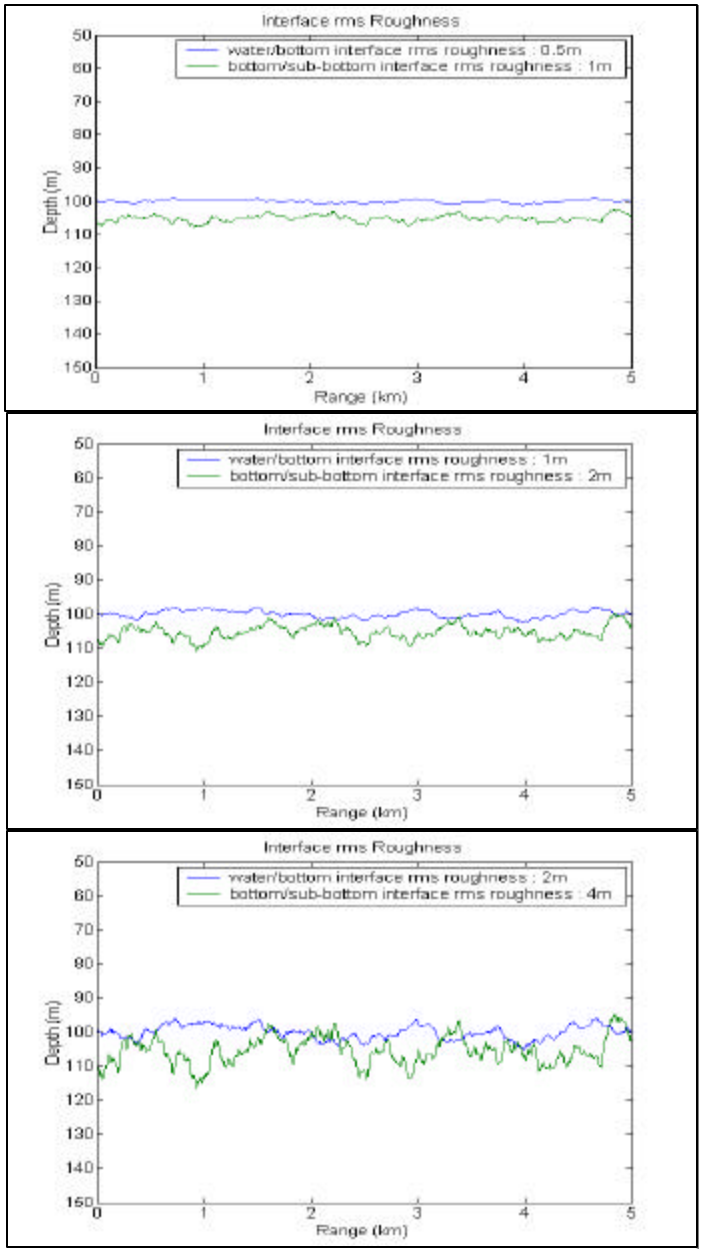


Figure 4. Plots of Different Interface Roughness

From Figure 4, increased roughness is observed as the rms values are increased. The longer wavelength perturbation also become more prominent with increased rms roughness. It is also observed that the largest rms roughness values (2m, 4m pair) produce some sub-bottom protrusions through the water/bottom interface. It should be noted that the vertical depth scale is in meters and the horizontal range scale is in kilometers, which makes the plots look extremely rough. The (1m, 2m) pair is used in the reference model.

### 3. Variations in Volume Perturbations

In order to depict a softer bottom layer covering a harder sub-bottom layer, the sound speed used in the bottom layer is 1700m/s while that of the sub-bottom layer is 1760m/s. This is typical of a sand/mud layer covering a gravel/rock sub-layer. The rms volume sound speed perturbations chosen are 5m/s, 15m/s and 45m/s. The 15m/s rms sound speed perturbation is the reference parameter.

The effects of the volumetric rms perturbation to the sound speed are illustrated in the figures on the next page. Apparent from the plots is the increasing contrast in the sound speed profile for an increasing volume sound speed perturbation. The rms sound speed perturbation of 15m/s is used in the reference model. It is not likely that the volume sound speed profile would vary considerably due to inhomogeneities and mixture of different sediment types as in the case with rms sound speed perturbation of 45m/s. However, the rms sound speed perturbation of 45m/s is still used for comparison purposes.

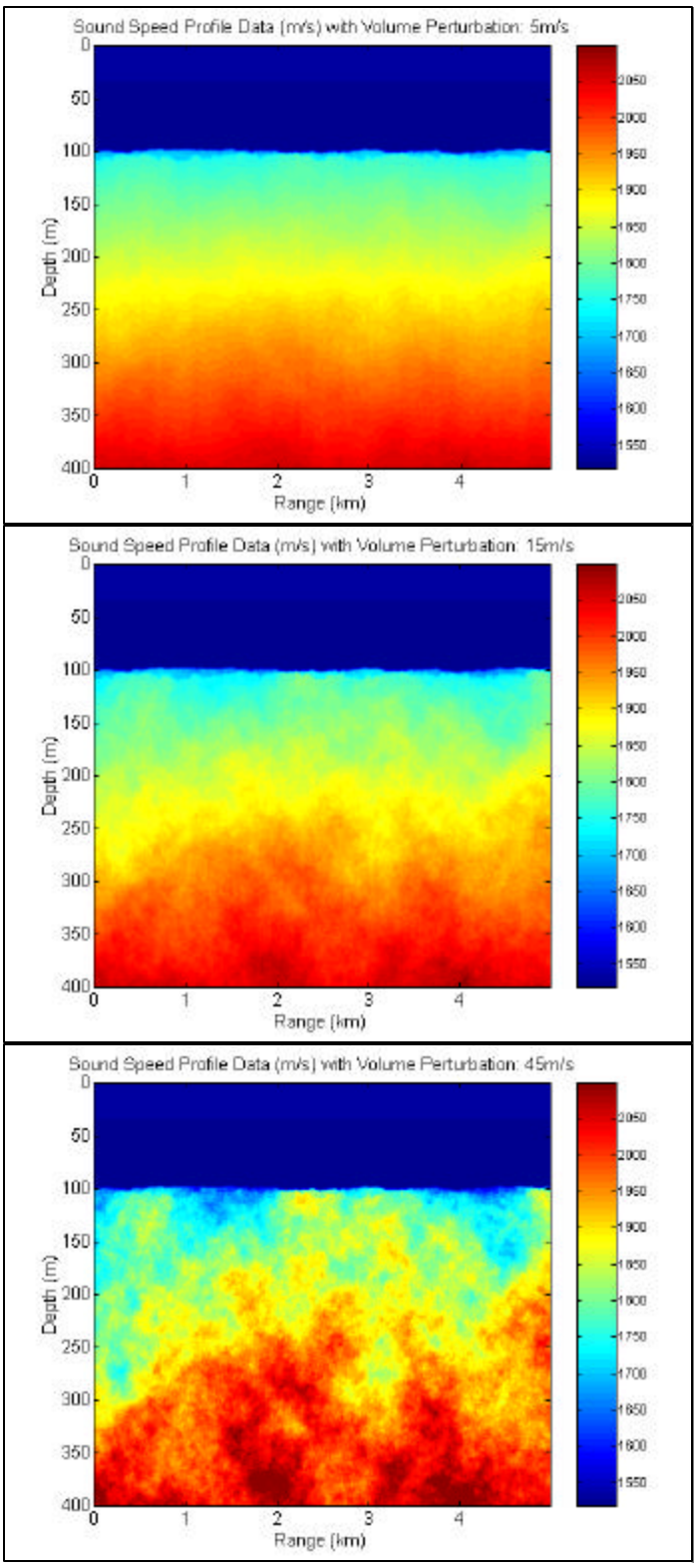


Figure 5. Plots of Sound Speed Data with Variations in Volume Perturbations

The differences in each environmental profile are summarized in the Table 1.

| Environmental Profiles | Sound Speed Profiles | Interface Roughness (rms) | | Bottom Volume Sound Speed Perturbation (rms) | Category |
|---|---|---|---|---|---|
| | | Water/ Bottom | Bottom/ Sub-Bottom | | |
| 1 | SSPAvg | 1m | 2m | 15m/s | Reference Model |
| 2 | SSP1 | 1m | 2m | 15m/s | Variations in Sound Speed |
| 3 | SSP2 | 1m | 2m | 15m/s | Variations in Sound Speed |
| 4 | SSPAvg | 0.5m | 1m | 15m/s | Variations in Interface Roughness |
| 5 | SSPAvg | 2m | 4m | 15m/s | Variations in Interface Roughness |
| 6 | SSPAvg | 1m | 2m | 5m/s | Variations in Volume Perturbations |
| 7 | SSPAvg | 1m | 2m | 45m/s | Variations in Volume Perturbations |

Table 1. Environmental Profiles

## 4. Other Parameters

The other parameters used in execution of the MMPE model, with their respective resident input filenames are specified below:

| Filename/Parameter | Value | Remarks |
|---|---|---|
| Main Control File: pefiles.inp | | |
| Number of depth points | 256 | Radix-2 integer required for FFT |
| Minimum depth | 0 m | |
| Maximum depth | 400 m | |
| Number of range steps | 833 | |
| Minimum range | 0 m | |
| Maximum range | 5.0 km | |
| Range step size | 6 m | |
| Maximum computed depth | 400 m | |
| Reference sound speed | 1500 m/s | |
| Source File: pesrc.inp | | |
| Source depths | Varying | Array elements at 20, 24, 28, 32, 36, 40, 44, 48, 52, 56, 60, 64, 68, 72, 76 and 80 m depths. |
| Center frequency | 250 Hz | |
| Frequency bandwidth | 250 Hz | |
| No. of Frequencies | 512 | Radix-2 integer required for FFT |
| Sound Speed File: pessp.inp | | |
| Water column sound speed | 3 sets | SSP1, SSP2 and SSPAvg<br>Range independent |
| No. of SSPs points | 58 | |
| Bathymetry: pebath.inp | | |

| Filename/Parameter | Value | Remarks |
|---|---|---|
| Mean bottom depth | 100 m | Range independent |
| No. of depth points | 1 | |
| Bottom properties: pebotprop.inp | | |
| Bottom sound speed | 1700 m/s | |
| Sound speed gradient | 1 /s | |
| Relative density | 1.6 | No density variation |
| Compressional attenuation | 0.15 dB/km/Hz | |
| Shear speed | 0 | Negligible |
| Shear attenuation | 0 | Negligible |
| Sub-Bottom Bathymetry: pedbath.inp | | |
| Depth | 105 m | |
| Sub-Bottom Properties: pedbotprop.inp | | |
| Sub-bottom sound speed | 1760 m/s | |
| Sound speed gradient | 1 | |
| Relative density | 2 | No density variation |
| Compressional attenuation | 0.2 dB/km/Hz | |
| Shear speed | 150 | |
| Shear attenuation | 0.5 | |
| RMS Perturbations (input during running of model) | | |
| Water/bottom interface roughness | 3 sets | 0.5m, 1m, 2m |
| Bottom/sub-bottom interface roughness | 3 sets | 1m, 2m, 4m |
| Volume sound speed fluctuation | 3 sets | 5m/s, 15m/s 45m/s |

Table 2. Input Environmental Parameters

THIS PAGE INTENTIONALLY LEFT BLANK

# IV. POST-PROCESSING AND RESULTS

## A. POST-PROCESSING 1 – TRANSMISSION LOSS

Before examining the two-way reverberation results, it is useful to examine the one-way transmission loss plots for the various environmental profiles to provide a preliminary examination of what may be expected. The transmission loss plots were based on propagation of CW signal with frequency of 250Hz from a source at 48m depth.

### 1. Transmission Loss Due to Variations in Sound Speed Profiles

The transmission loss plots for the three different sound speed profiles were very similar in structure. Hence, there should be little variation in the reverberation loss. It is noted that energy is being refracted upwards in the sub-bottom layer. This is due to the sound speed gradient of 1m/s/m included in the sub-bottom layer.

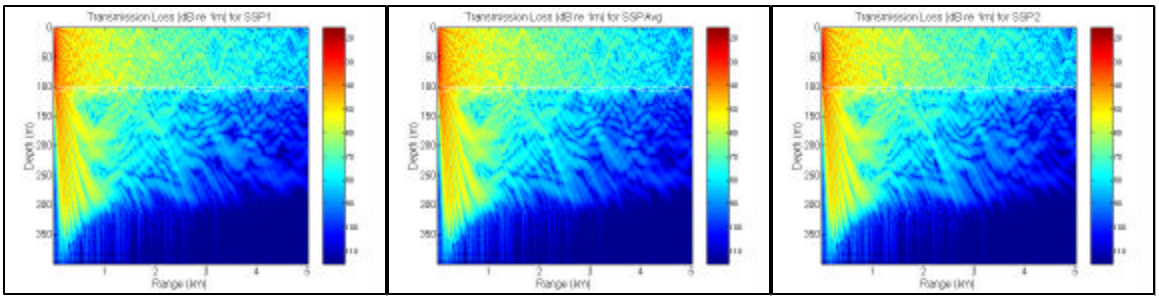

Figure 6. Transmission Loss Due to Variations in Sound Speed Profiles

### 2. Transmission Loss Due to Variations in Interface Roughness

The transmission loss structures for the three different sets of interface roughness look similar, as seen in Figure 7. However, careful observation shows that the higher interface rms roughness values have lower transmission loss. This may be because the higher roughness values have caused the sediment layer between the water/bottom and the bottom/sub-bottom interfaces to be thinner and allow the acoustic energy to interact more readily with the denser and faster volume below the bottom/sub-bottom interface. Thus, more forward propagation of the energy occurs. In the case of the largest roughness values, the sub-bottom protrusions through the water/bottom interface may have cause even greater forward propagation of the energy. Therefore, lower

reverberation loss (or higher reverberation level) for higher interface rms roughness values may be expected.

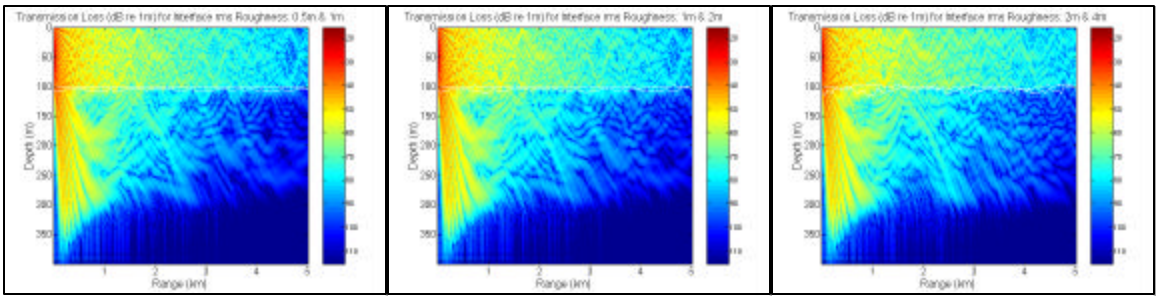

Figure 7. Transmission Loss Due to Variations in Interface Roughness

### 3. Transmission Loss Due to Variations in Volume Perturbations

It is observed that the transmission loss is greatly affected by the variations in volume perturbations. The high sound speed fluctuation value of 45m/s increases the transmission loss significantly. The transmission loss from the 15m/s volume sound speed fluctuation is also considerably higher than that of the 5m/s fluctuation. In an attempt to determine the cause, the sound speed data plot from Figure 5 is examined. It is found that at short ranges there is a patch of slower bottom sound speed between 0 and 0.3km. This patch of slower bottom sound speed has allowed more of the signal to penetrate the bottom.

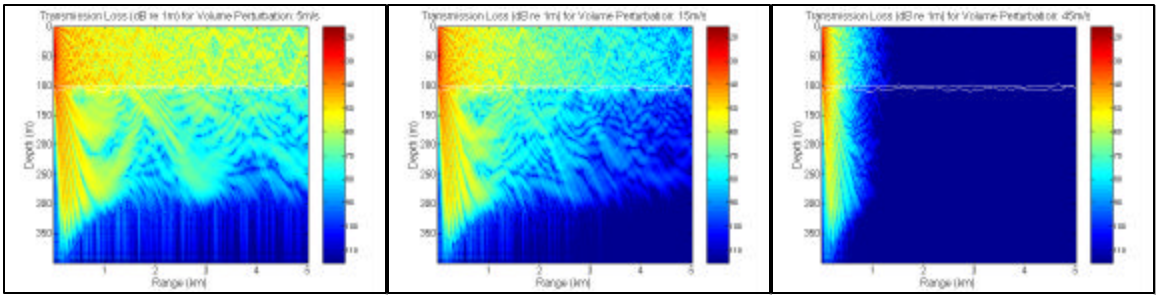

Figure 8. Transmission Loss Due to Variations in Volume Perturbations

In order to further examine the high transmission loss created by the high volume sound speed fluctuation, the model is run with a new random seed to create a different bottom sound speed profile (Figure 9) with a sound speed fluctuation of 45m/s. It is found that at short ranges (0 to 0.3km), the bottom sound speed profile is slightly higher than the previous. The transmission loss plot also shows lower transmission loss out to

that range. Note that there is another slow patch further out (about 0.6km to 1km) that causes high transmission loss at a further range. This confirms that a high volume sound speed fluctuation may create a slow bottom that significantly reduces reflection, thus increasing transmission loss. We should then expect to see high reverberation loss at high volume sound speed fluctuation. It should be noted that the rest of the results and analysis in the following sections are based on the original sound speed profile data created by the original seed.

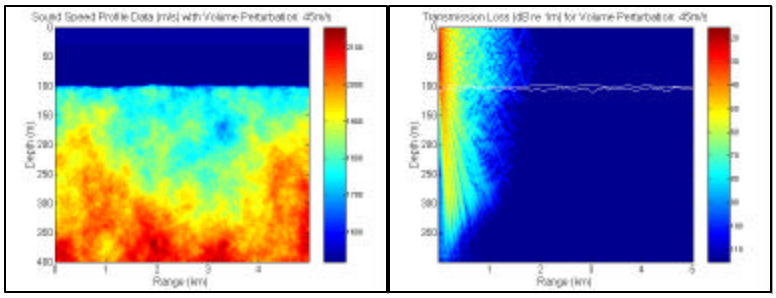

Figure 9. Sound Speed Profile Data and Transmission Loss for New Random Seed

## B. POST-PROCESSING 2 - REVERBERATION LOSS

### 1. Time Domain Reverberation Analysis

To evaluate the bottom reverberation loss, analyses of the pulse propagation in the time-domain for both the reverberation structure of the interface and volume were necessary. The time-domain analyses were previously explained in Chapter II, Section D. The equations required to formulate the MATLAB implementation for the interface and the volume reverberation loss are summarized below:

- For the interface reverberation loss, $RL_b$,

$$p_{2-way,b}(r_m, f) = p_{+Tb}(r_m, f)\, p_{+Rb}(r_m, f), \tag{4.1}$$

$$\Rightarrow \quad p_{-b}(r_m, t) = \int p_{2-way,b}(r_m, f) e^{-i2\pi ft} df, \tag{4.2}$$

$$\Rightarrow \quad p_{-b}(t_n) = \sum_{m=1}^{M} p_{-b}(r_m, t_n), \tag{4.3}$$

$$\Rightarrow \quad RL_b(t_n) = -20\log\left[\left|p_{-b}(t_n)\right|\right]. \tag{4.4}$$

- For the volume reverberation loss, $RL_v$,

$$p_{2-way,v}(r_m, z, f) = n(r_m, z)\, p_{+T}(r_m, z, f)\, p_{+R}(r_m, z, f), \tag{4.5}$$

$$\Rightarrow \quad p_{2-way,v}(r_m, z, t) = \int p_{2-way,v}(r_m, z, f) e^{-i2\pi ft} df, \tag{4.6}$$

$$\Rightarrow \quad p_{-v}(r_m, t) = \int_{z>z_b}^{\infty} p_{2-way,v}(r_m, z, t)\, dz, \tag{4.7}$$

$$\Rightarrow \quad p_{-v}(t_n) = \sum_{m=1}^{M} p_{-v}(r_m, t_n), \tag{4.8}$$

$$\Rightarrow \quad RL_v(t_n) = -20\log\left[\left|p_{-v}(t_n)\right|\right]. \tag{4.9}$$

## 2. Reference Model Reverberation Loss

With a source depth of 48m, the general color maps of the water/bottom and bottom/sub-bottom interfaces and volume reverberation losses (for 2-way transmission) were obtained from the reference model (Figure 10). Fine multipath structures due to the interface and volume fluctuations were present. Careful observation shows that the arrival times of the first signal returns occur earlier at the receiver at 80m, while the latest arrive at the receiver at 20m. This was due to the shorter distance between the deeper receiver and the bottom, thus receiving returns earlier than the shallower receivers. The color map of the bottom/sub-bottom interface reverberation loss shows a few maxima and minima.

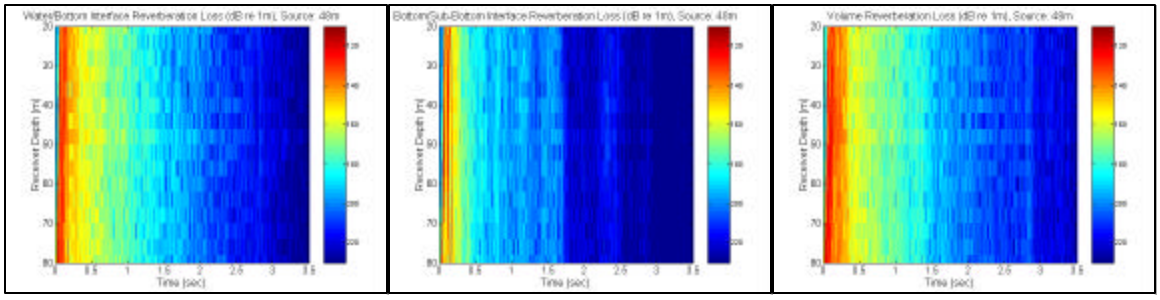

Figure 10. Color Maps of Reference Model Reverberation Loss

With the receiver chosen at 40m depth, the water/bottom interface reverberation and volume reverberation plots are shown in Figure 11. The plots have rather similar structure. The bottom/sub-bottom interface reverberation has a few conspicuous maxima and minima not observed in the other curves. This is due to the sound speed gradient included in the sub-bottom layer, which causes the energy to be refracted upwards and interact with the bottom/sub-bottom interface.

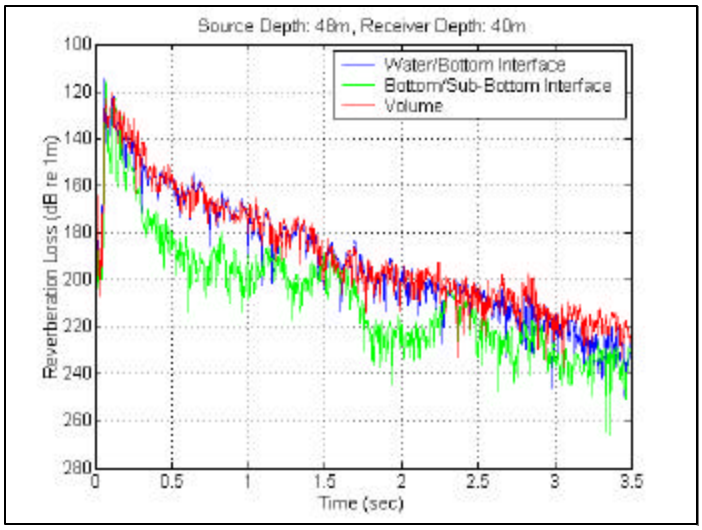


Figure 11. Reference Model Reverberation Loss

### 3. Reverberation Loss Due to Variations in Sound Speed Profiles

The reverberation loss color maps for the different sound speed profiles show very similar structures. This is probably due to the relatively small variations between the sound speed profiles.

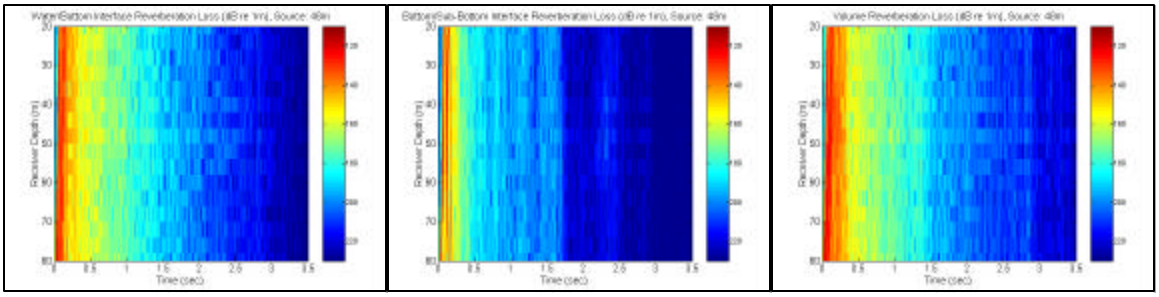

Figure 12. Color Maps of Reverberation Loss Due to SSP1

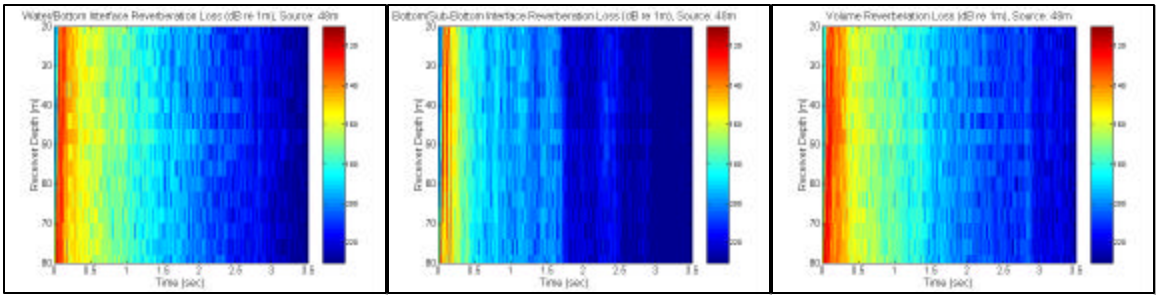

Figure 13. Color Maps of Reverberation Loss Due to SSPAvg

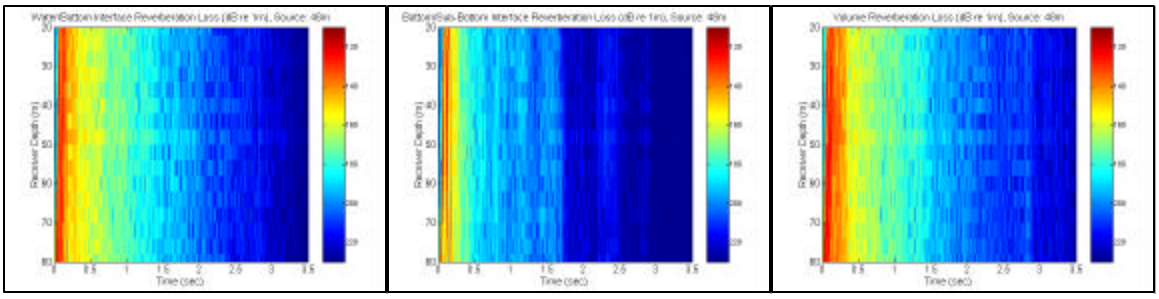

Figure 14. Color Maps of Reverberation Loss Due to SSP2

With the receiver at 40m depth, the reverberation loss structures for the 3 sound speed profiles are seen to be quite similar. This is consistent with the color maps.

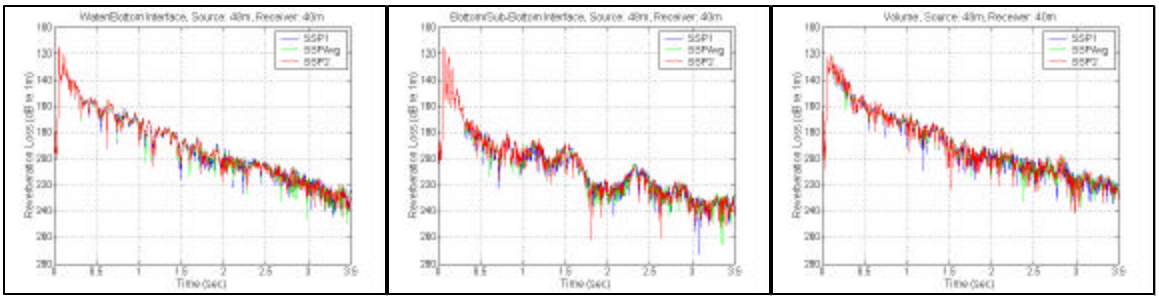

Figure 15. Reverberation Loss Due to Variations in Sound Speed Profiles

## 4. Reverberation Loss Due to Variations in Interface Roughness

The reverberation color maps look similar for the different values of interface rms roughness. But when observed carefully, the color maps from the bottom/sub-bottom interface reverberation display a more obvious difference, with the higher roughness values producing higher reverberation levels. As explained earlier, this may be because the higher roughness values cause the sediment layer between the water/bottom and the bottom/sub-bottom interfaces to be thinner and allow the acoustic energy to interact more readily with the denser and faster volume below the bottom/sub-bottom interface.

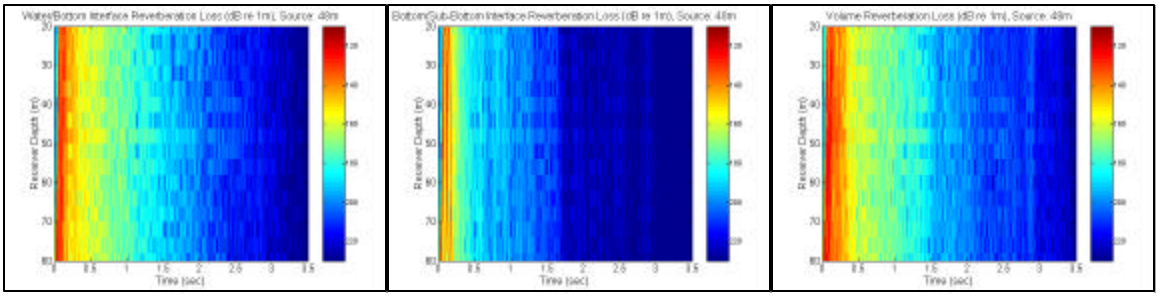

Figure 16. Color Maps of Reverberation Loss due to Water/Bottom and Bottom/Sub-Bottom Interface rms Roughness of 0.5m and 1m Respectively

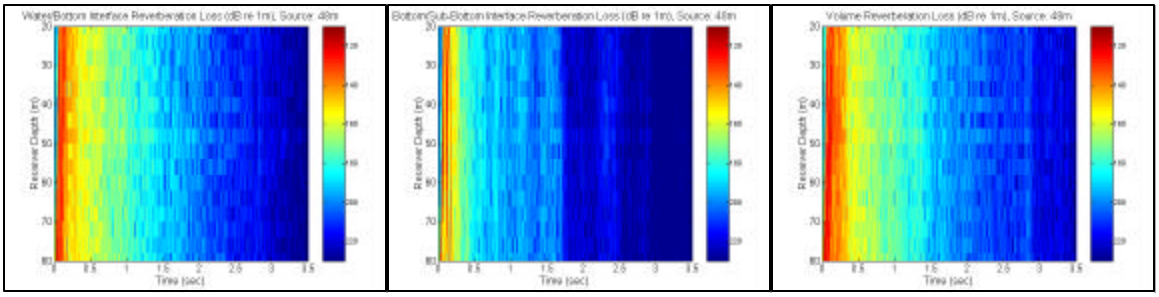

Figure 17. Color Maps of Reverberation Loss due to Water/Bottom and Bottom/Sub-Bottom Interface rms Roughness of 1m and 2m Respectively

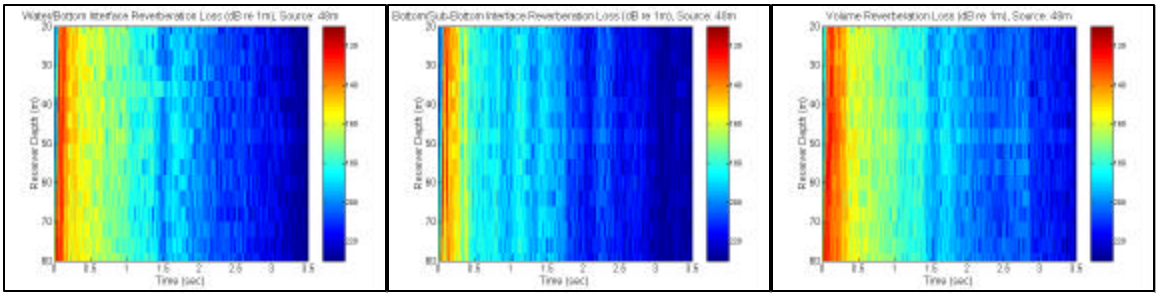

Figure 18. Color Maps of Reverberation Loss due to Water/Bottom and Bottom/Sub-Bottom Interface rms Roughness of 2m and 4m Respectively

The effect of the variations in interface rms roughness is not very prominent in the water/bottom interface and volume reverberation loss, though both showed that the higher rms values produce slightly higher reverberation level. However, this effect can be seen most clearly from the bottom/sub-bottom interface where the higher interface rms roughness produces reverberation levels which are about 10dB higher. This is probably caused by the bottom/sub-bottom interface being nearer the water volume at higher roughness values. This allows more energy to interact with the denser and faster sub-bottom volume, hence, creating more reverberation.

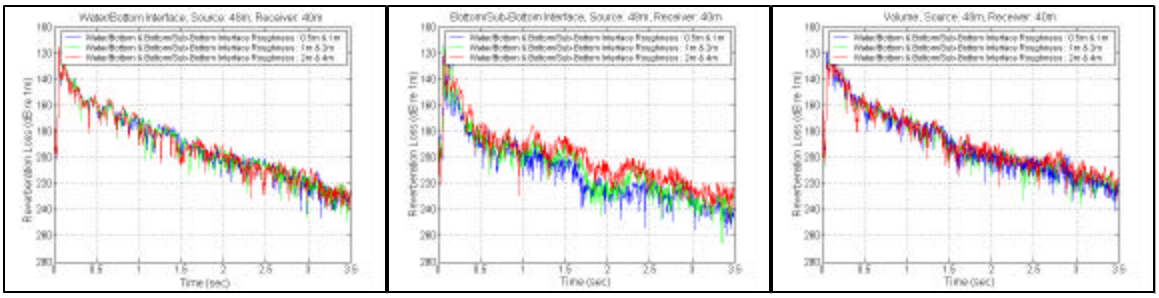

Figure 19. Reverberation Loss Due to Variations in Interface Roughness

## 5. Reverberation Loss Due to Variations in Volume Perturbations

It is very obvious from the color maps that an increase in volume rms sound speed perturbation reduces the reverberation level for the water/bottom, bottom/sub-bottom interfaces and the volume. The reduced reverberation level arising from the increase in volume sound speed fluctuations is most probably caused by the patch of slower bottom sound speed at short ranges, which allows more energy to penetrate the bottom. This is consistent with the transmission loss results.

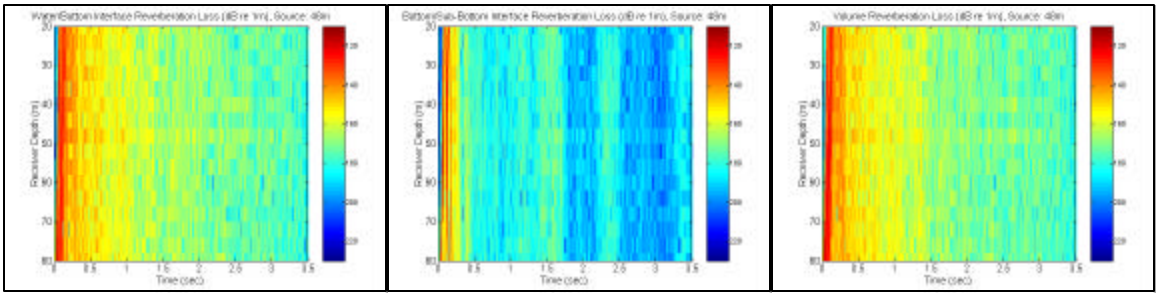

Figure 20. Color Maps of Reverberation Loss Due to Volume Perturbation with rms Sound Speed Fluctuation of 5m/s

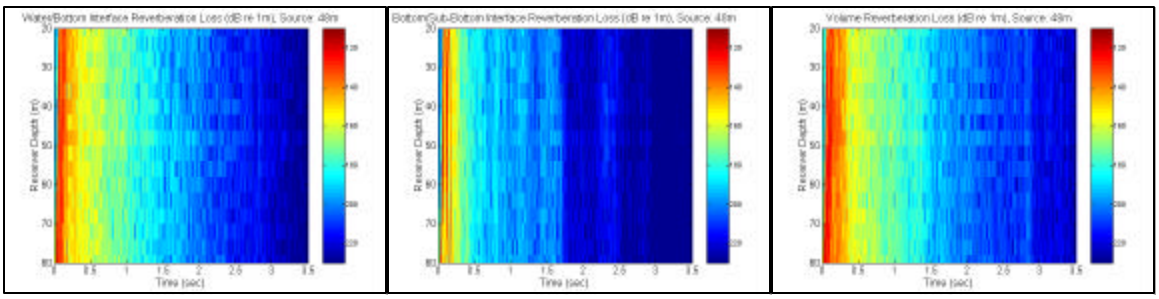

Figure 21. Color Maps of Reverberation Loss Due to Volume Perturbation with rms Sound Speed Fluctuation of 15m/s

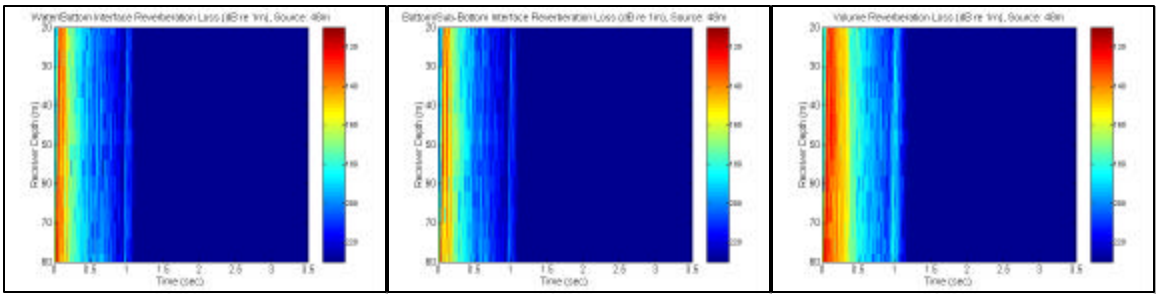

Figure 22. Color Maps of Reverberation Loss Due to Volume Perturbation with rms Sound Speed Fluctuation of 45m/s

The reverberation plots with receiver at 40m depth show that the reverberation level is significantly reduced as the volume rms sound speed perturbation is increased, which is consistent with the color maps. As explained earlier, this is probably the result of more energy penetrating the patch of slower bottom sound speed at short ranges.

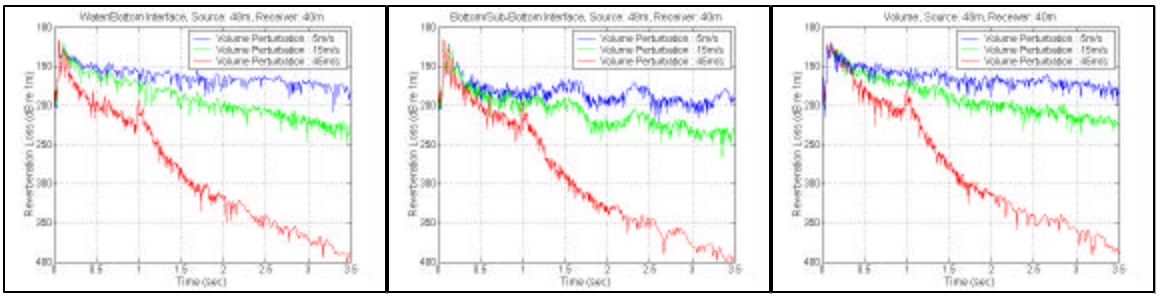

Figure 23. Reverberation Loss Due to Variations in Volume Perturbations

## C. POST-PROCESSING 3 - VERTICAL CORRELATIONS

As we are dealing with broadband signals, the vertical correlations for interface and volume reverberation were computed in the time-domain.

### 1. Vertical Correlation Due to Variations in Sound Speed Profiles

The color maps of the vertical correlation for the different sound speed profiles show very similar structure. It is observed that the reverberation from the bottom/sub-bottom interface decorrelates fastest, followed by reverberation from the water/bottom interface and then the volume. From the color maps, it can also be seen that the deeper receivers are receiving signals earlier than the shallower receivers, thus resulting in the positive time lag with reference to the source at 48m.

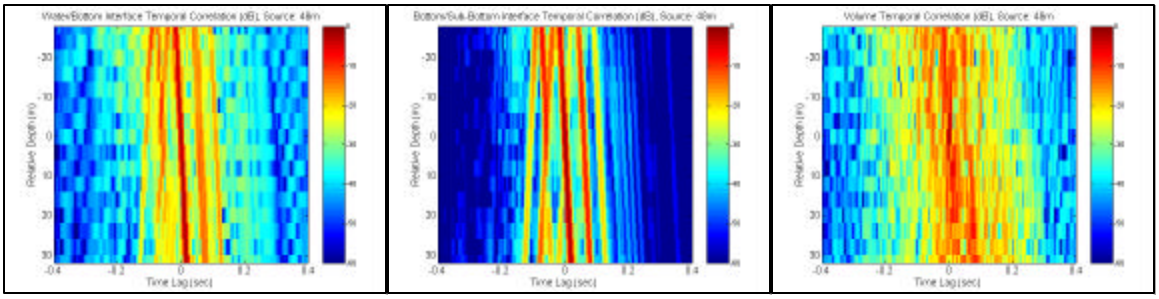

Figure 24. Vertical Correlation Due to SSP1

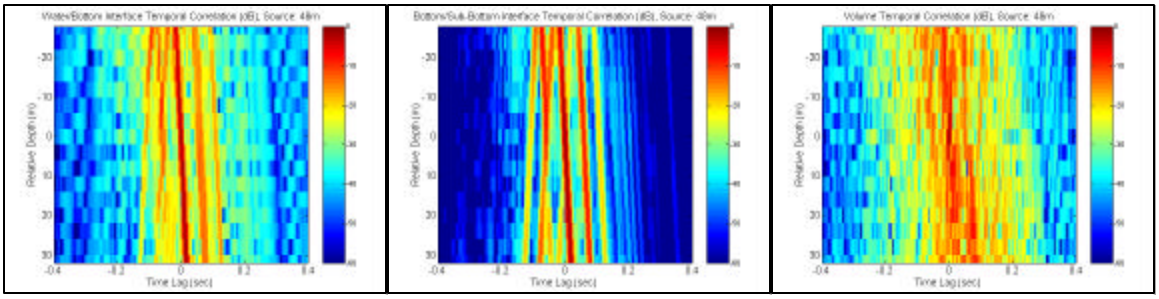

Figure 25. Vertical Correlation Due to SSPAvg

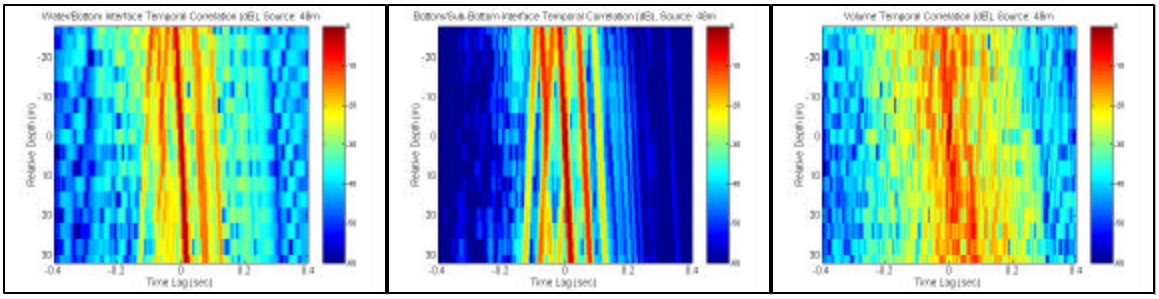

Figure 26. Vertical Correlation Due to SSP2

### 2. Vertical Correlation Due to Variations in Interface Roughness

From the color maps, it is noted that the reverberation from the bottom/sub-bottom interface decorrelates the fastest across time, followed by the water/bottom interface, then the volume, as was observed for the variations in sound speed profiles. The various structures look rather similar when comparing the various rms roughness values with the exception of the bottom/sub-bottom interface, which shows a prominent difference. The bottom/sub-bottom interface reverberation displays that an increase in the vertical correlation with an increase in the rms roughness. This may be because more energy is interacting with the bottom/sub-bottom interface as the rms roughness is increased, as previously described.

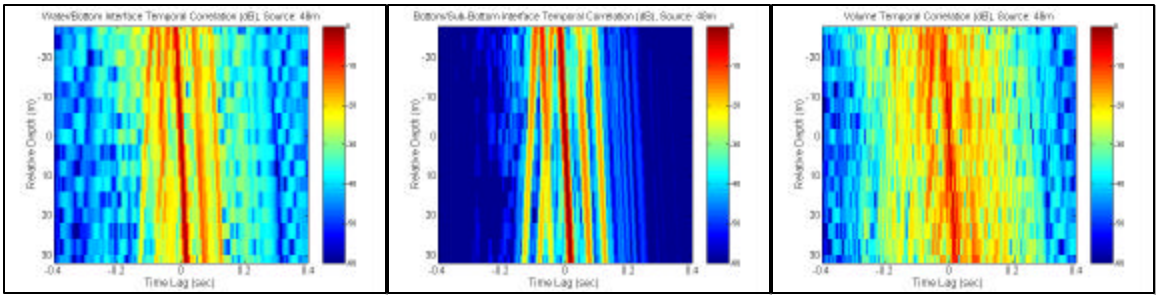

Figure 27. Vertical Correlation due to Water/Bottom and Bottom/Sub-Bottom Interface rms Roughness of 0.5m and 1m Respectively

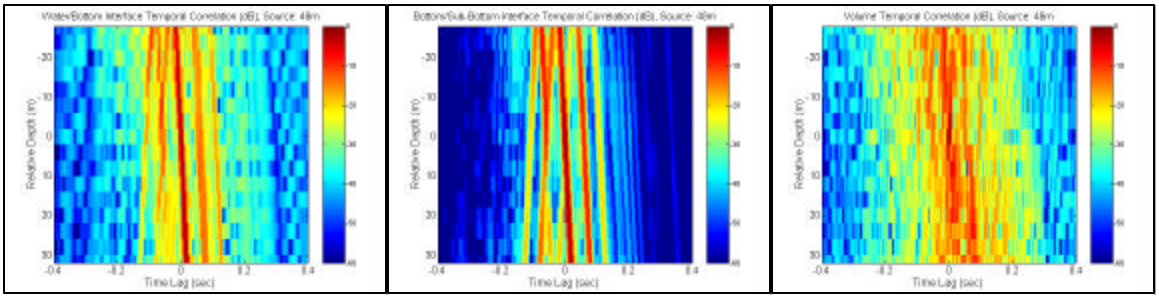

Figure 28. Vertical Correlation due to Water/Bottom and Bottom/Sub-Bottom Interface rms Roughness of 1m and 2m Respectively

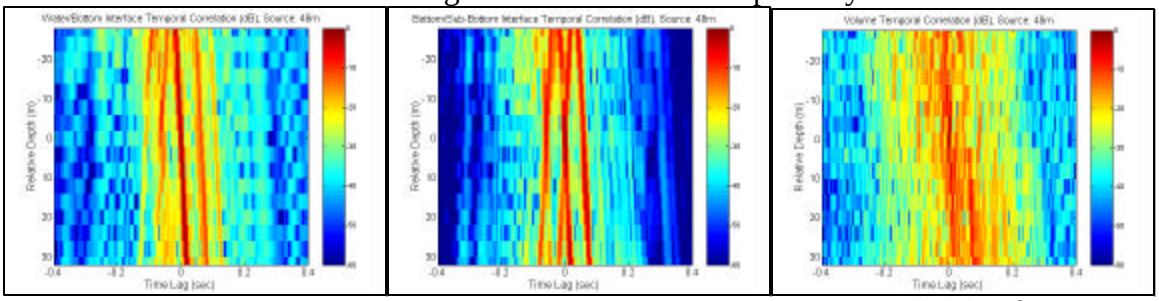

Figure 29. Vertical Correlation due to Water/Bottom and Bottom/Sub-Bottom Interface rms Roughness of 2m and 4m Respectively

### 3. Vertical Correlation Due to Variations in Volume Perturbations

From the color maps, it is observed that the reverberation decorrelates fastest over time when the volume sound speed perturbation is increased. This is true for all reverberation types, the water/bottom and bottom/sub-bottom interfaces and the volume. It is seen that the reverberation from the bottom/sub-bottom interface decorrelates the fastest, followed by the water/bottom interface and then the volume, as before.

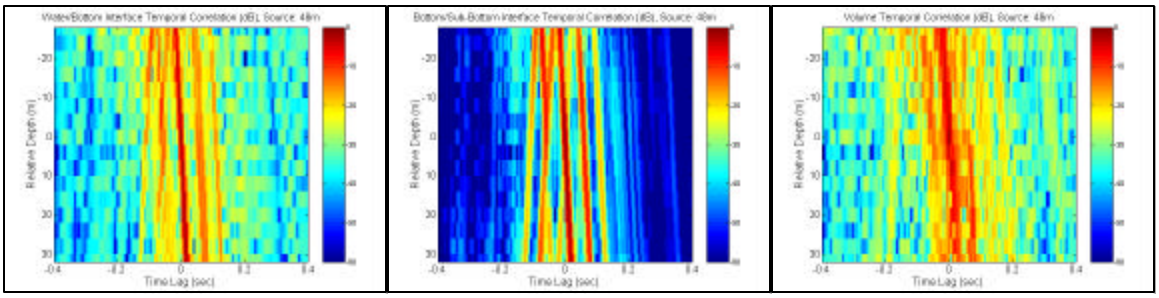

Figure 30. Vertical Correlation Due to Volume Perturbation with rms Sound Speed Fluctuation of 5m/s

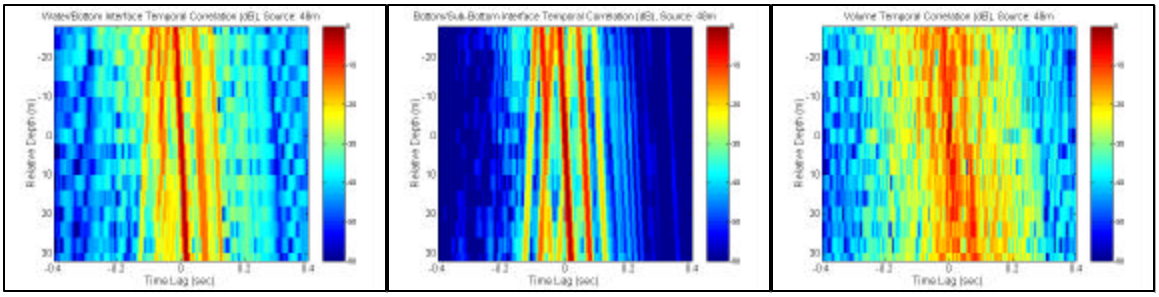

Figure 31. Vertical Correlation Due to Volume Perturbation with rms Sound Speed Fluctuation of 15m/s

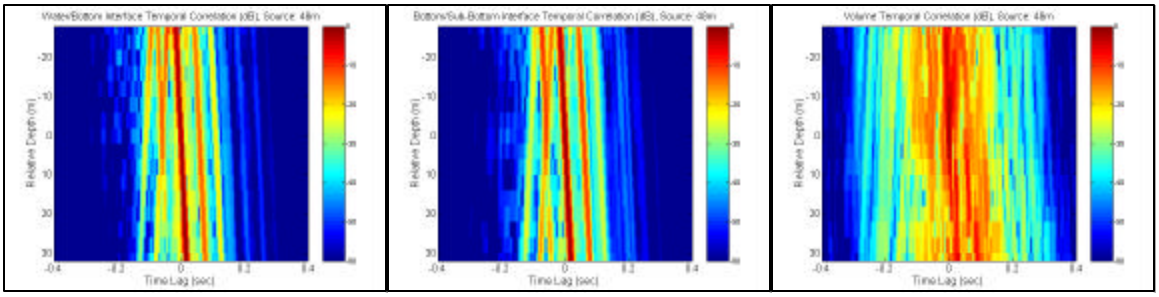

Figure 32. Vertical Correlation Due to Volume Perturbation with rms Sound Speed Fluctuation of 45m/s

## D. POST-PROCESSING 4 – PEAK VERTICAL CORRELATION

In this section, the peak correlation values were extracted from the vertical correlation of the previous section in order to see how the signals decorrelate across depth.

### 1. Peak Vertical Correlation of Reference Model

From the figure below, it is seen that volume reverberation decorrelates the fastest over depth. The bottom/sub-bottom interface reverberation shows better correlation initially but is consistent with the water/bottom interface reverberation when the source/receiver separation is increased.

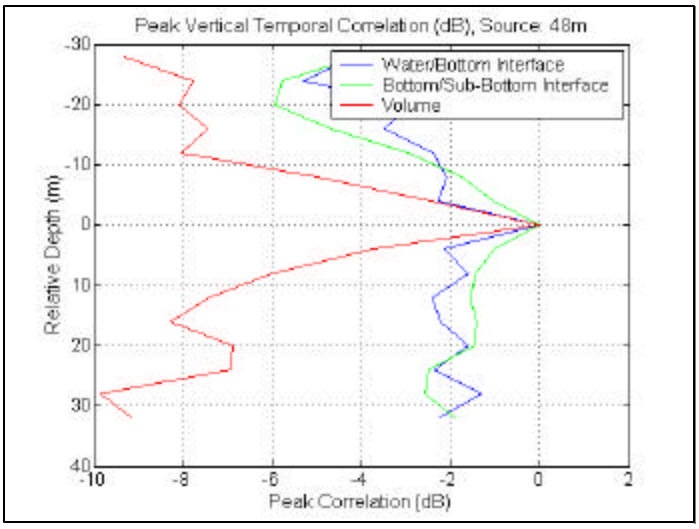


Figure 33. Peak Vertical Correlation of Reference Model

### 2. Peak Vertical Correlation Due to Variations in Sound Speed Profiles

The peak vertical correlation structures for various sound speed profiles are very similar. Thus, the influence of the water coulum sound speed variability on reverberation coherence appears to be minimal.

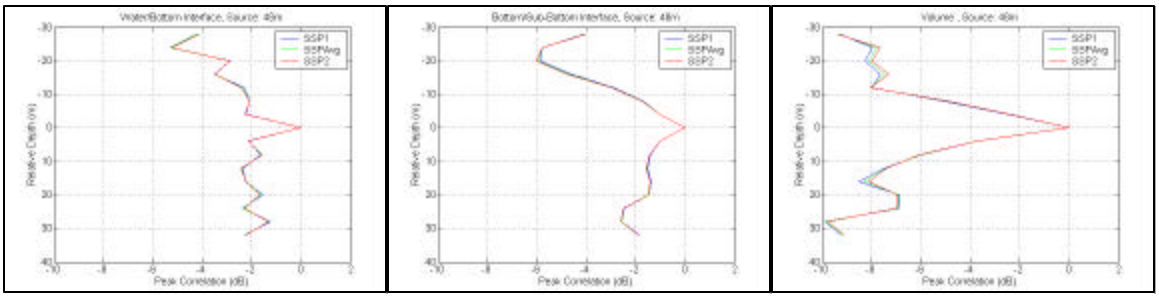

Figure 34. Peak Vertical Correlation Due to Variations in Sound Speed Profiles

### 3. Peak Vertical Correlation due to Variations in Interface Roughness

The peak vertical correlation curves for the water/bottom interface due to the different interface rms roughness have only slight differences in their structures. However, for the bottom/sub-bottom interface, the reverberation decorrelates more rapidly for increased interface roughness. It seems that the increase in interface roughness has caused the vertical coherence of the bottom/sub-bottom interface to be lost in the volume. As for the volume reverberation, the decorrelation rate was somewhat affected by changes in the interface roughness, but not to the same degree and not consistently.

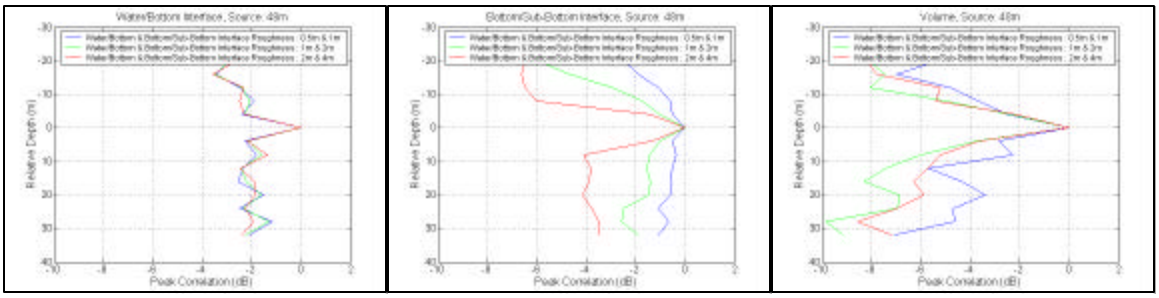

Figure 35. Peak Vertical Correlation Due to Variations in Interface Roughness

### 4. Peak Vertical Correlation Due to Variations in Volume Perturbations

For the case of the water/bottom and bottom/sub-bottom interface reverberation, the smaller the volume sound speed perturbation, the faster the decorrelation rate. However, the increase in vertical correlation for large volume perturbations is not due to a true increase in structural coherence but rather a significant decrease in reverberation levels. In other words, if no signal is received, then it will correlate very well with itself but has no physical significance. For the volume reverberation, the rate of decorrelation was not affected as much or as consistently.

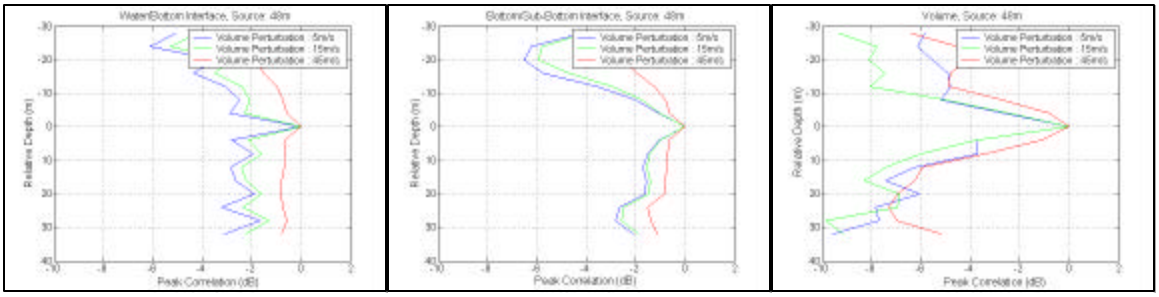

Figure 36. Peak Vertical Correlation Due to Variations in Volume Perturbations

## E. POST-PROCESSING 5 – POWER SPECTRAL DENSITY

In order to extract the spectral components of the reverberation data for the broadband signals, the *power spectral density (PSD)* and *power ratio spectral density (PRSD)* were computed. The PRSD analysis will be discussed in the next section. The magnitude-squared of the ranged-reduced reverberation was analyzed using the Discrete Fourier Transform (DFT), such that the PSD is defined by[1]

$$PSD = DFT\left\{\left|p_{-}\right|^{2}.\left|r\right|^{2}\right\}, \tag{4.10}$$

where $p$- is the reverberation field of the interface or volume. It should be noted that the time-domain pressure field is first converted to range dependent data by the use of the reference sound speed $c_0$ , such that range = time x $c_0$.

### 1. PSD of Reference Model

The PSD plot shows a gradual drop in normalized power in the lower wavenumber of up to about $0.1\text{m}^{-1}$ (about 60m length scale) for the interface and volume reverberations. After that, a significant drop-off in normalized power was observed. The spectral slope over the length scales of 60m to 600m is about -0.55, while the slope over the length scales of 10m to 60m is about –1.7.

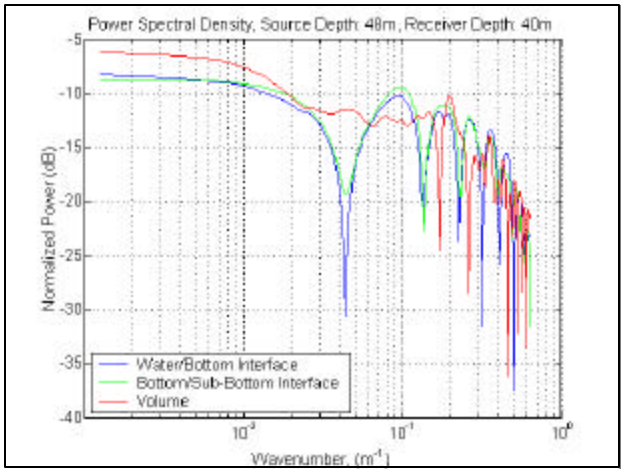


Figure 37. Power Spectral Density of Reference Model

### 2. PSD Due to Variations in Sound Speed Profiles

The PSD structures for the various sound speed profiles are very similar to one another for the interface and volume reverberations. Only minor deviation is observed for the volume reverberation. Thus, the effects of water column sound speed variations on the signal statistics appear to be minimal.

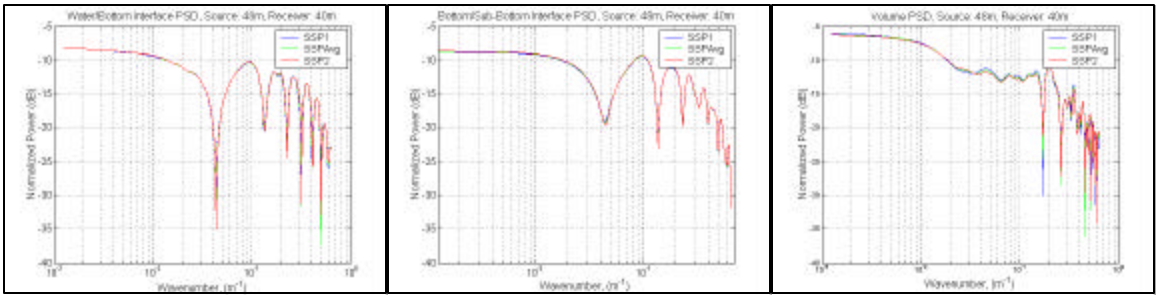

Figure 38. Power Spectral Density Due to Variations in Sound Speed Profiles

### 3. PSD Due to Variations in Interface Roughness

The water/bottom interface reverberation PSD plot shows little deviation due to different levels of interface roughness. The bottom/sub-bottom interface reverberation PSD plot shows that the higher interface rms roughness produces slightly higher normalized power at wavenumber up to about $0.2m^{-1}$ (about 30m length scale), after which the lower interface rms roughness contributes to higher normalized power at the drop-off. For volume reverberation, the higher interface rms roughness consistently produces lower normalized power throughout. This may be due to the energy interacting more with the rougher interface causing more forward propagation, and less energy is interacting with the volume.

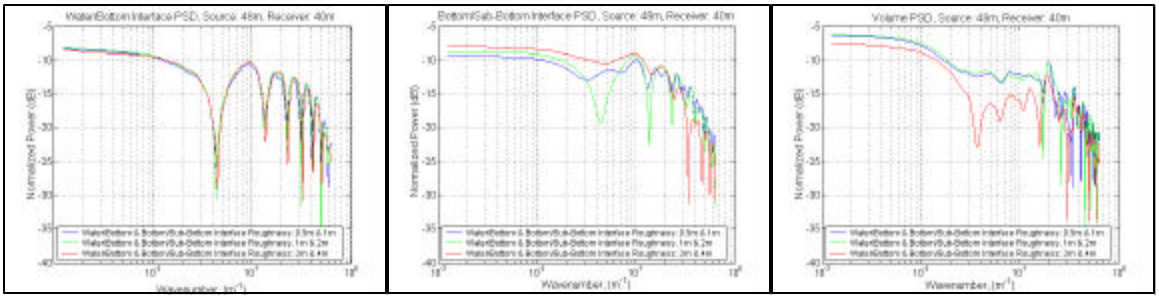

Figure 39. Power Spectral Density Due to Variations in Interface Roughness

### 4. PSD due to Variations in Volume Perturbations

The water/bottom interface reverberation produces normalized power which decreases with an increase in volume sound speed perturbation, though the 5m/s and 15m/s rms sound speed perturbation show minor deviation. The structures of the bottom/sub-bottom interface reverberation PSD plot are similar to that of the water/bottom interface. The PSD structures produced by the volume reverberation are different. The rms sound speed perturbation of 15m/s produces higher normalized power for most wavenumber scales except from $0.02m^{-1}$ to $0.2m^{-1}$(length scales of about 30m to 300m). The normalized power from the 45m/s rms sound speed perturbation is consistently lower throughout as may be expected from the transmission loss analysis.

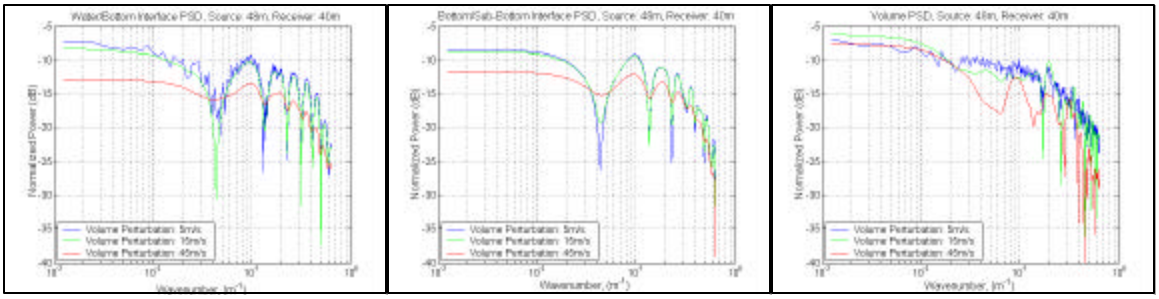

Figure 40. Power Spectral Density due to Variations in Volume Sound Speed Perturbations

## F. POST-PROCESSING 6 – POWER RATIO SPECTRAL DENSITY

In order to further examine spectral content, the power ratio spectral density (PRSD) was implemented. The PRSD is defined in terms of the ratio of the reverberation filed of a particular model to that of the unperturbed model, specifically[1]

$$PRSD = DFT\left\{\frac{\left|p_{\text{perturbed}}\right|^2}{\left|p_{\text{unperturbed}}\right|^2}\right\} \tag{4.11}$$

where $p_{\text{perturbed}}$ is the reverberation field of the interface or volume of the model of interest and $p_{\text{unperturbed}}$ is the reverberation field of the reference model without interface roughness and volume fluctuations.

### 1. PRSD of Reference Model

The PRSD of the reference model shows varying results from the water/bottom interface, bottom/sub-bottom interface and volume. The bottom/sub-bottom interface shows the strongest normalized power, followed by the volume and then the water/bottom interface. The normalized power of the bottom/sub-bottom fluctuates significantly, followed by the water/bottom interface and then the volume. Over the length scales of 10m to 60m, the response of the bottom/sub-bottom interface has a steeper slope of about –0.3 compared to a slope of about –0.2 for bottom/sub-bottom interface and volume.

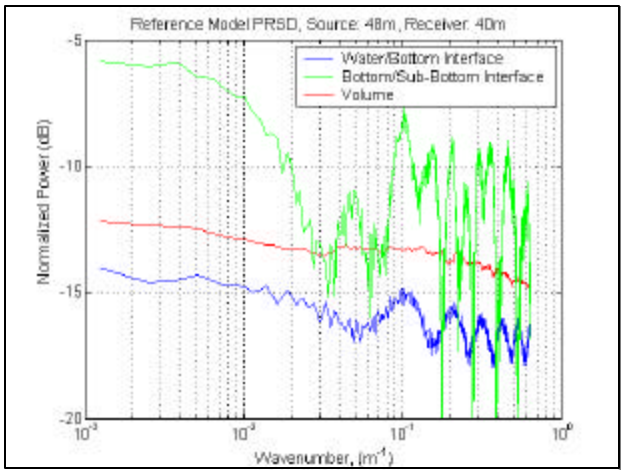


Figure 41. Power Ratio Spectral Density of Reference Model

### 2. PRSD due to Variations in Sound Speed Profiles

The PRSD structures of the interfaces and volume show little difference due to the variations in the sound speed profiles of the water column. As before, this suggests that the effect of the different sound speed profiles is minimal.

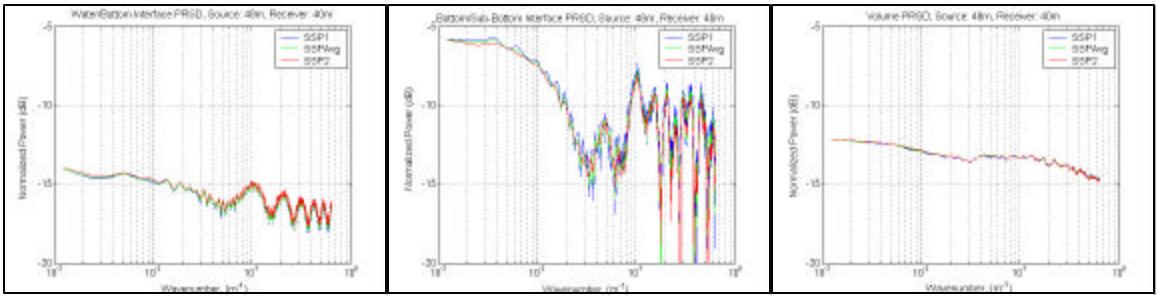

Figure 42. Power Ratio Spectral Density Due to Variations in Sound Speed Profiles

### 3. PRSD Due to Variations in Interface Roughness

The PRSD due to different levels of interface roughness show varying results. At the water/bottom interface, the PRSDs have about the same normalized power, although the fluctuation is greater with the higher interface roughness. At the bottom/sub-bottom interface, the higher interface roughness value produces higher normalized power, which is consistent with the transmission loss result. The volume PRSD shows lesser fluctuation with the highest normalized power produced by the interface roughness pairs (1m, 2m) followed by (2m, 4m) then lastly (0.5m, 1m).

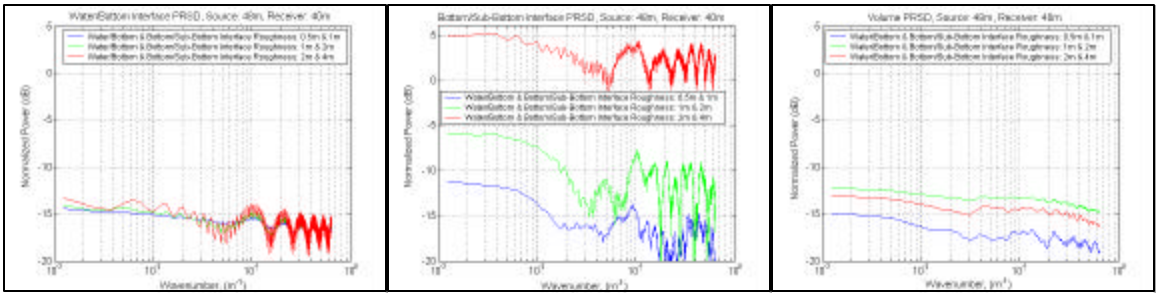

Figure 43. Power Ratio Spectral Density due to Variations in Interface Roughness

### 4. PRSD Due to Variations in Volume Perturbations

The variations in volume perturbations produce significantly different PRSD. At the water/bottom interface, the normalized power is highest with the sound speed perturbation of 45m/s. The 5m/s and 15m/s sound speed perturbations produce about the same magnitude of normalized power, except that there is a significant fluctuation with the 5m/s sound speed perturbation. This is not consistent with the transmission loss result and the cause is not known at this time. At the bottom/sub-bottom interface, the 5m/s sound speed perturbation has the highest normalized power, followed by the 15m/s and then the 45m/s sound speed perturbations. In this case, the result is consistent with the transmission loss analysis, where the loss is greatest at higher volume perturbation. In the volume, higher sound speed perturbation produces higher normalized power, and the 5m/s sound speed perturbation shows greater fluctuation than the other two. Again, this is not consistent with the transmission loss result.

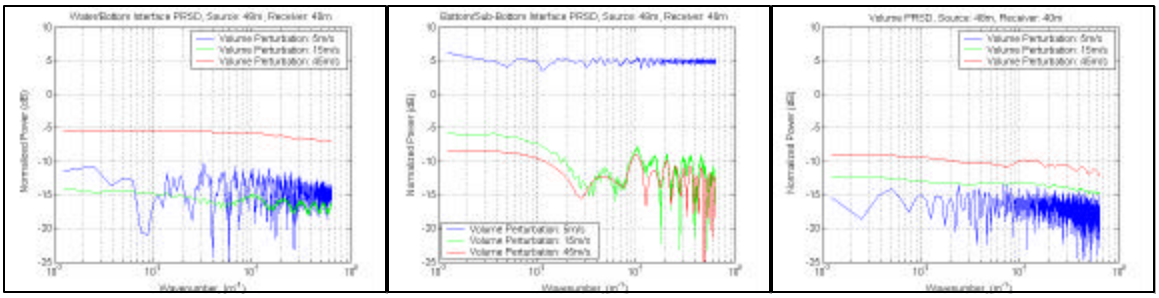

Figure 44. Power Ratio Spectral Density Due to Variations in Volume Perturbations

THIS PAGE INTENTIONALLY LEFT BLANK

# V. SUMMARY

The main focus of this thesis was to investigate the influence of different environmental profiles on the reverberation structures due to the water/bottom interface, bottom/sub-bottom interface and bottom/sub-bottom volume. Simulations were conducted using the same reverberation geometry and environmental parameters as defined in previous work. A vertical line array (VLA) with 16 elements was chosen to provide the reverberation measurements and computations. The source was located at a depth of 48m with all 16 elements receiving the reverberation. Seven different environmental models were used in the computation and were summarized in Table 1. The main differences among the seven models were the water column sound speed profile, interface roughness and volume perturbation. Of the seven profiles, one was chosen as the reference model with which the others were compared. Several analyses such as reverberation pressure levels, vertical correlation, peak correlation and spectral characteristics were performed using broadband signals.

The transmission loss analysis provided a good preliminary prediction of what would be expected in the reverberation level analysis. It was found the three different sound speed profiles did not show much difference in the transmission loss. As for the variations in the interface roughness, the rougher interface produced less transmission loss, i.e. the signal was able to propagate further. This may be because the higher roughness values have caused the sediment layer between the water/bottom and the bottom/sub-bottom interfaces to be thinner and allow the acoustic energy to interact more readily with the denser and faster volume below the bottom/sub-bottom interface. Thus, more forward propagation of the energy occurs. However, the higher volume perturbation increased the transmission loss significantly. This was probably due to the higher chances of producing a relatively slower bottom, thus, allowing the signal to penetrate more readily and not be reflected back into the water column.

The variations in sound speed profiles of the water column showed little difference in the reverberation levels, correlation and spectral analyses. The variations in interface roughness showed that a rougher interface produced higher reverberation levels

and higher normalized power in the power spectral analysis. This was consistent with the transmission loss analysis. In general, vertical correlation analysis relative to a source depth at 48m showed that the volume decorrelates much faster followed by the bottom/sub-bottom interface, then the water/bottom interface. It was also noted that the higher interface roughness caused the peak vertical coherence of the bottom/sub-bottom interface to be lost in the volume. The variations in volume perturbations showed that the higher sound speed perturbation produced lower reverberation levels and lower normalized power in the power spectral analysis, which was consistent with the transmission loss result. There was no significant difference in the correlation analysis for the different volume perturbations, except when a large rms value was used. In the PRSD analysis, higher normalized power was generated by higher volume perturbation. There was no clear connection of this result with the transmission loss result at this time.

With the conclusion of this thesis, recommendations for future work are :

- To perform short-range statistical analysis to narrow down the relationship between signal structure and environmental structure. This is an attempt to interpret influence of multipath effects on long-range structures.
- To perform vertical correlation analysis using a range of pulse lengths. This may help to distinguish interface from volume reverberation structures.
- To incorporate environmental measurements from actual ASIAEX data and conduct prediction analysis.
- To conduct data processing of ASIAEX data and perform data/model comparisons.
- To incorporate rough sea surface scatter into the propagation model and investigate influence on various reverberation level predictions.

# LIST OF REFERENCES


[1] Li, L.S. "Parabolic Equation Modeling of Bottom Interface and Volume Reverberation in Shallow Water," Master's Thesis, Naval Postgraduate School, Monterey, CA, September 2000.

[2] Kao, H. "Numerical Analysis of Bottom Reverberation and Influence of Density Fluctuations," Master's Thesis, Naval Postgraduate School, Monterey, CA, December 2001.

[3] Smith, K.B. "Convergence, stability, and variability of shallow water acoustic predictions using a split-step Fourier parabolic equation model," *J. Comp. Acoust*., Volume 9, Number 1, September 1999.

[4] Dahl, P. H. "ASIAEX, East China Sea, Cruise Report of the Activities of the R/V Melville 29 May to 9 June 2001," Applied Physics Laboratory, University of Washington, Seattle, WA, July 2001.

[5] Hardin, R. H. and Tappert, F. D. "Applications of the split-step Fourier method to the numerical solution of nonlinear and variable coefficient wave equations," SIAM Rev. 15, 1973.

[6] Goff, J.A. and Jordan, T.H. "Stochastic modeling of seafloor morphology: Inversion of Sea Beam data for second-order statistics," *J. Geophys. Res. 93*, 1988.

[7] Yamamoto, T. "Velocity variabilities and other physical properties of marine sediments measured by crosswell acoustic tomography," *J. Acoust. Soc. Am*., Volume 98 (4), 1995.

[8] Smith, K.B. "Incorporation of Density Fluctuations in Sediment," Lecture Notes, 2001.

[9] Smith, K.B. and Cushman, E.B. "A comparison of quasi-continuous wave and broadband travel time techniques in the prediction of long-range reverberation," *J. Acoust. Soc. Am*., Volume 102, 1997.

[10] Smith, K.B. and Tappert, F.D. "UPME: The University of Miami Parabolic Equation Model Version 1.1," MPL Technical Memorandum 432, San Diego, CA, 1994.

[11] Tappert, F. D. "The parabolic approximation method," in Lecture Notes in Physics, Vol. 70, Wave Propagation and Underwater Acoustics, edited by J. B. Keller and J. S. Papadakis (Springer-Verlag, New York, 1977).

[12] Thomson, D.J. and Chapman, N.R. "A wide-angle split–step algorithm for the parabolic equation," *J. Acoust. Soc. Am.*, Volume 74, 1983.

[13] Jensen, F.B., Kuperman, W.A., Porter, M.B., Schmidt, H. Computational Ocean Acoustics ( Springer-Verlag New York, Inc., 2000).

[14] Urick, R.J. *Principles of Underwater Sound, Third Edition* (McGraw-Hill, Inc., 1993).

# INITIAL DISTRIBUTION LIST

1. Defense Technical Information Center
   Ft. Belvoir, Virginia

2. Dudley Knox Library
   Naval Postgraduate School
   Monterey, California

3. Prof. Kevin B. Smith (Code PH/Sk)
   Department of Physics
   Naval Postgraduate School
   Monterey, California

4. Dr. Jeff Simmen (Code 321OA)
   Office of Naval Research
   Arlington, Virginia

5. Dr. Ellen Livingston (Code 321OA)
   Office of Naval Research
   Arlington, Virginia